Latest Smithian (Early Triassic) ammonoid assemblages in Utah (western USA basin) and their implications for regional biostratigraphy, biogeography and placement of the Smithian/Spathian boundary.

Arnaud Brayard, James F. Jenks, Kevin G. Bylund, Nicolas Olivier, Emmanuelle Vennin, Daniel A. Stephen, Gilles Escarguel, Emmanuel Fara

Latest Smithian (Early Triassic) ammonoid assemblages in Utah (western USA basin) and their implications for regional biostratigraphy, biogeography and placement of the Smithian/Spathian boundary

Arnaud Brayard [1,*], James F. Jenks [2], Kevin G. Bylund [3], Nicolas Olivier [4], Emmanuelle Vennin [1], Daniel A. Stephen [5], Gilles Escarguel [6], Emmanuel Fara [1]

[1] Biogéosciences, UMR6282, CNRS, Université Bourgogne Franche-Comté, 6 Boulevard Gabriel, 21000 Dijon, France

[2] 1134 Johnson Ridge Lane, West Jordan, Utah 84084, USA

[3] 140 South 700 East, Spanish Fork, Utah 84660, USA

[4] Université Clermont Auvergne, CNRS, Laboratoire Magmas et Volcans, 63000 Clermont-Ferrand, France

[5] Department of Earth Science, Utah Valley University, 800 West University Parkway, Orem, Utah 84058, USA

[6] Univ Lyon, Université Claude Bernard Lyon 1, CNRS, ENTPE, UMR 5023 LEHNA, F-69622, Villeurbanne, France

* Corresponding author. E-mail address: arnaud.brayard@u-bourgogne.fr (A. Brayard).

Abstract

The late Smithian extinction represents a major event within the Early Triassic. This event generally corresponds to a succession of two and possibly three successively less diverse, cosmopolitan ammonoid assemblages, which when present, provide a robust biostratigraphic framework and precise correlations at different spatial scales. In the western USA basin, known occurrences of latest Smithian taxa are rare and until now, have only been documented from northeastern Nevada. Based on these restricted basinal occurrences, a regional zone representing the latest Smithian was postulated but not corroborated, as representative taxa had not yet been reported from outside Nevada. Here we document two new ammonoid assemblages from distant localities in northern Utah, overlying the late Smithian *Anasibirites* beds and characterized by the unambiguous co-occurrence of *Xenoceltites subevolutus* and *Pseudosageceras augustum*. The existence of a latest Smithian zone in the western USA basin is therefore validated, facilitating the identification of the Smithian/Spathian boundary and intra-basin correlation. This zone also correlates with the latest Smithian zone recognized from southern Tethyan basins. Additionally, these new data support other observed occurrences of *Xenoceltites subevolutus* throughout most of the late Smithian.

Keywords:

Late Smithian, Early Triassic, Ammonoids, Utah, Biostratigraphy

1. Introduction

The Early Triassic represents a time of marked successive biological and environmental changes following the Permian/Triassic mass extinction (PTME; ~252 Ma; Baresel et al., 2017). This ~5 myr-long period is for instance associated with major fluctuations in oceanic temperatures, global carbon cycle and anoxic conditions presumably triggered by the Siberian Traps (Payne et al., 2004; Galfetti et al., 2007; Sun et al., 2012; Grasby et al., 2013; Romano et al., 2013; Zhang F. et al., 2018; Thomazo et al., 2019; Zhao et al., 2020), although evidence for such a link has not yet been firmly established for all known environmental fluctuations (Widmann et al., 2020). Several secondary extinction events occurred during the Early Triassic, including a severe one at the onset of the late Smithian and continuing through the interval containing the Smithian/Spathian boundary (SSB; ~249.2 Ma; Tozer, 1982; Dagys, 1988; Brayard et al., 2006; Orchard, 2007; Hermann et al., 2012; Zhang L. et al., 2019). With regard to its effect on ammonoids, this event, which may be almost equal in magnitude to the PTME (Jattiot et al., 2016), is associated with a change in spatial distribution of taxa, becoming highly cosmopolitan (e.g., Brayard et al., 2006, 2007), and experiencing a drastic reduction in disparity (e.g., Brosse et al., 2013). The late Smithian event is coeval to a marked cooling following a temperature maximum reached near the middle/late Smithian boundary (e.g., Goudemand et al., 2019). In some localities, associated deposits also show probable dysoxic to anoxic environments (e.g., Galfetti et al., 2008; Grasby et al., 2013; Brayard et al., 2019), although the exact location of this anoxia between the water column and the sediment remain to be elucidated. Mechanisms underlying the late Smithian extinction are still unexplained (Widmann et al., 2020) but our knowledge of this event has improved recently. It shows that successive cosmopolitan ammonoid assemblages thrived during the late Smithian cooling (Jenks et al., 2015; Jattiot et al., 2016), although it is expected that they would become more endemic when influenced by such climatic trend

(Brayard et al., 2006). Nevertheless, an overall understanding of the numerous consecutive biotic and abiotic phenomena taking place at that time still requires their placement in a robust biostratigraphic framework in order to provide precise correlations at different spatial scales.

Early Triassic biostratigraphical scales based on ammonoids (e.g., Smith, 1932; Spath, 1934) and produced prior to the beginning of the 2010s (e.g., Tozer, 1994; Ermakova, 2002; Brayard and Bucher, 2008) have often treated the late Smithian as a unique biostratigraphic entity with numerous genera of the family Prionitidae, such as *Anasibirites* and *Wasatchites*, considered as typical of this time interval. However, in the last decade, many works have shown that the late Smithian can be subdivided into at least two parts (Brühwiler et al., 2010a, 2011, 2012a, b; Brayard et al., 2013; Jattiot et al., 2017; Jenks and Brayard 2018; see Jenks et al., 2015 for a summary of late Smithian global correlations). The lower part corresponds to a marked worldwide dominance of prionitids, a species-rich family (Jattiot et al., 2016), associated with a few xenoceltitid species (e.g., *Xenoceltites subevolutus*) and rare occurrences of surviving arctoceratids, inyoitids, galfettitids and palaeophyllitids in some places (Brühwiler et al., 2012a, b; Shigeta and Kumagae, 2015; Smyshlyaeva et al., 2018; Jattiot et al., 2020; questionably in Tozer, 1994, and Piazza et al., 2017). In most regions (see Zakharov et al., 2013, in press, for a putative exception regarding late Smithian ammonoid assemblages from deep-water facies of South Primorye, which enigmatically appear relatively dissimilar and more diverse than elsewhere), the Prionitidae abruptly disappeared prior to the onset of the upper part that is characterized by the occurrence of assemblages, in which latest Smithian representatives of xenoceltitids (*Glyptophiceras*, *Xenoceltites*, *Condensoceras*) and hedenstroemiids (e.g., *Pseudosageceras augustum*, *P. plicatum, ?P. bullatum*) coexist (e.g., Brühwiler et al., 2012a; Jattiot et al., 2017; Jenks and Brayard, 2018). Very few of these taxa survived the SSB, but at least two other families (the proptychitids and palaeophyllitids)

virtually persisted into the Spathian (Brayard and Bucher, 2015; see also Zakharov et al., in press, for another surviving scheme based on a different phylogenetic conception).

In the western USA basin, where known occurrences of latest Smithian taxa are rare, the SSB is most often placed within the interval of separation between the late Smithian *Anasibirites* beds and the early Spathian *Bajarunia-Tirolites* beds (see Brayard et al., 2019 for a review of index taxa and correlations within this basin). Thus, the recognition of the SSB in this basin is often proposed with some temporal uncertainties. Until now, ammonoid species characterizing the second part of the late Smithian (e.g., *Pseudosageceras augustum, Condensoceras youngi, Glyptophiceras sinuatum*) were indeed firmly documented from Palomino Ridge (Jattiot et al., 2017) and Crittenden Springs (Jenks et al., 2010; Jenks and Brayard, 2018), northeastern Nevada, even though they are of prime importance for location of the SSB. Finally, a third zone potentially representing the very end of the late Smithian, and thus corresponding to a putative third part, has been newly reported from northeastern Nevada (Widmann et al., 2020). Taxa found in this unique worldwide assemblage are still undescribed but apparently correspond to intermediate forms between late Smithian *Xenoceltites* and early Spathian *Bajarunia*, *Tirolites* and *Columbites* (Widmann et al., 2020). Pending a detailed description of this new assemblage and its stratigraphic position, we consider the assemblages including *P. augustum*, *C. youngi* and *G. sinuatum* as "latest Smithian" in age.

Based on these restricted basinal occurrences, and especially on the presence of *P. augustum*, Jattiot et al. (2017) postulated the existence of a regional Unitary Association Zone (their UAZ6) representing the second part of the late Smithian. To corroborate the existence of this zone throughout the western USA basin, representatives of *P. augustum*, *Condensoceras* or *Glyptophiceras* must therefore be reported from outside Nevada. A few specimens described as Hedenstroemiidae gen. indet. A, and resembling *P. augustum*, were

described from the Xenoceltitidae gen. indet. A beds of central Utah (Brayard et al., 2013). However, their poor state of preservation prevented a firm determination and the confirmation of the presence of latest Smithian ammonoid assemblages outside Nevada. Mathews (1929) also reported the existence of specimens closely resembling *Glyptophiceras* ("*Xenodiscus hannai*" in Mathews, 1929: pl. 1:1-4) and *P. augustum* ("*Cordillerites compressus*" in Mathews, 1929: pl. 1:15-17; "*P. intermontanum*" in Mathews, 1929: pl. 1:18-22) in the Fort Douglas area, north-central Utah. However, he never published a detailed stratigraphy showing the relative placement of each sampled taxon, but instead most often referred to coexistences within a stratigraphic unit corresponding to several beds with prionitid assemblages. We therefore strongly suspect that assemblages corresponding to the second part of the late Smithian can also be found in this area, but a complete bed-by-bed re-sampling work remains necessary to validate this hypothesis.

Here we report two new ammonoid assemblages from distant localities in northern Utah, overlying the late Smithian *Anasibirites* beds and characterized by the unambiguous co-occurrence of *Xenoceltites subevolutus* and *Pseudosageceras augustum*. These assemblages support the existence of a regional zone (UAZ6 of Jattiot et al., 2017) representing the second part of the late Smithian in the western USA basin. When present, this zone facilitates the identification of the SSB and intra-basin correlation. It also correlates with the latest Smithian zone recognized from southern Tethyan basins.

2. Exposures and sampled material

The western USA basin was located within the northern intertropical zone on the western margin of the Panthalassa during the Early Triassic (Fig. 1(A)). Its sedimentary deposits presently outcrop across a wide area including Utah, northern Arizona, eastern Nevada, southeastern Idaho, western Wyoming, and southwestern Montana (Fig. 1(B)). The

two studied exposures are located in northern Utah (Fig. 1(C)). They exhibit classical shale-limestone alternations of the Early Triassic Thaynes Group (*sensu* Lucas et al., 2007), which represent relatively shallow sedimentary deposits in an epicontinental sea. The maximum extent of this epicontinental sea within the western USA basin occurred during the Smithian–Spathian transition (Lucas et al., 2007; Brayard et al., 2013, 2020; Vennin et al., 2015; Olivier et al., 2018) and was probably controlled by a North-South differentiation in regional tectonics (Caravaca et al., 2018) and by concurrent global climatic changes (e.g., Brayard et al., 2020).

Smithian ammonoid assemblages were sampled in Tooele and Morgan Counties, northern Utah (Fig. 1(C)). At both sites, ammonoid preservation is highly variable but is generally good, with test parts remaining on some specimens. Similar to many other ammonoid localities in Utah (Brayard et al., 2020), internal recrystallization is common, making the preparation of these fragile specimens often difficult. However, the extent of recrystallization at these sites is sometimes rather fine, allowing the observation of suture lines on a few specimens.

The Lower Weber Canyon locality (LWC; Figs. 1(C), 2; 41°3'50.86"N, 111°34'0.02"W – WGS84 coordinates) is located in Morgan County along Interstate Highway 84 and the Weber River. It was first mapped by Schick (1955) and Mullens and Laraway (1964), and then described by Smith (1969) who reported the occurrences of middle Smithian *Meekoceras* assemblages and late Smithian prionitids. Donovan (1986) and Yurchyk (2011) further studied some ammonoids and conodonts collected from this site for addressing specific taphonomic and geochemical issues, respectively. More recently, the LWC section was described in detail by Grosjean et al. (2018) for its lithological and sedimentological record. These authors show that unlike many other exposures of the Thaynes Group in the western USA basin, Microbially Induced Sedimentary Structures are present in middle

Smithian strata (Fig. 2: “Unit B”). They also highlighted that (*i*) late Smithian strata (Fig. 2: base of “Unit C”) correspond to a mid-ramp setting with frequent storm deposits and thus include bioclastic accumulations with densely packed ammonoids, and (*ii*) the SSB is concomitant to the maximum transgression in this area (Lucas et al., 2007; Brayard et al., 2013, 2020). Ammonoid specimens are abundant in the base of “Unit C” but sometimes fragmentary and slightly deformed. Sampled late Smithian ammonoid assemblages are typical from this time interval. A large ammonoid size spectrum is represented, ranging from less than 0.5 cm up to ~11 cm.

The second studied site is located on the southwestern end of Thumb Ridge (TR; Figs. 1(C), 3; 40°50'49.89"N, 113°11'17.35"W – WGS84 coordinates), located in Tooele County. Doelling et al. (1994) mapped this area and reported the occurrences of different Spathian assemblages, especially in ledge-forming limestones that are well exposed in the landscape. Underlying rocks were described by these authors as (*i*) containing sparse and poorly-preserved fossils, and (*ii*) corresponding to the “Dinwoody Fm.”, which is of ?Griesbachian-Dienerian age (e.g., Kummel, 1954, 1957). A recent mapping by Clark and Oviatt (2019) highlighted the presence of the middle Smithian *Owenites* beds and late Smithian *Anasibirites* beds, two informal biozones, thus indicating that these strata did not pertain to the Dinwoody Fm. Our concomitant investigations of the same strata led to the discovery of several relatively well-preserved ammonoid assemblages including characteristic late Smithian prionitids and xenoceltitids as well as the latest Smithian taxon *Pseudosageceras augustum*. Additionally, these rocks show typical alternating shale and limestone that are similar to several Thaynes Group exposures in Utah, thus supporting the fossil evidence that they do not belong to the Dinwoody Fm. Due to the high proportion of shales forming the area’s incompetent hills, fossiliferous limestones only sporadically crop out. Late Smithian ammonoids are densely clustered in storm bioclastic accumulations that resemble late

Smithian strata in LWC, thus suggesting a relatively similar depositional environments. Fragmentary ammonoids are often found, but some specimens are almost complete.

3. Systematic palaeontology

Systematic descriptions mainly follow the classification of Tozer (1981), and that further refined by Brayard et al. (2013, 2020), Jattiot et al. (2016, 2017) and Jenks and Brayard (2018). Quantitative morphological ranges for identified species are illustrated by scatter diagrams based on classical measurements of the diameter (D), and corresponding whorl height (H), whorl width (W) and umbilical diameter (U). Scatter diagrams of H, W and U, and H/D, W/D and U/D are provided only when the number of measured specimens is higher than four. Detailed measurements are given in Table S1 (Appendix A). The number of sampled specimens (fragmentary to complete) for each taxon and locality is indicated as "n =". Repository of figured specimens is abbreviated UBGD (Université de Bourgogne, Géologie Dijon, France). Abbreviations: TR: Thumb Ridge; LWC: Lower Weber Canyon.

Phylum Mollusca Linnaeus, 1758

Class Cephalopoda Cuvier, 1797

Subclass Ammonoidia Fischer, 1882

Order Ceratitida Hyatt, 1884

Superfamily Xenodiscoidea Frech, 1902

Family Xenoceltitidae Spath, 1930

Genus ***Xenoceltites*** Spath, 1930

Type species: *Xenoceltites subevolutus = Xenodiscus* cf. *comptoni* (non Diener) Frebold, 1930

Remarks: A thorough discussion of the different species attributed to *Xenoceltites,* as well as a comparison with some other late Smithian xenoceltitid genera was provided by Jattiot et al. (2017) and Jenks and Brayard (2018). Only a simplified description of *X. subevolutus* is therefore given below.

Xenoceltites subevolutus Spath, 1930

Fig. 4

?1929. *Ophiceras matheri* Mathews, p. 4, pl. 1, figs. 38-40.

?1929. *Xenodiscus douglasensis* Mathews, p. 5, pl. 1, figs. 5-7.

1930. *Xenoceltites subevolutus* Spath, p. 12.

1930. *Lecanites* cf. *L. ophioneus* – Frebold, p. 12, pl. 3, figs. 4, 4a, 5.

1930. *Xenodiscus* cf. *X. comptoni* – Frebold, p. 14, pl. 3, figs. 1-3.

?1932. *Xenodiscus rotula* – Smith, p. 45, pl. 79, figs. 5, 6 (copy of Mathew's 1929 figure and description of *X. matheri*).

1934. *Xenoceltites spitsbergensis* Spath, p. 128, pl. 9, figs. 1, 2; pl. 11, figs. 5, 7, 8.

1934. *Xenoceltites gregoryi* Spath, p.129, pl. 5, fig. 3; pl. 6, figs. 4, 5; pl. 11, figs. 3, 4, 6.

1934. *Xenoceltites subevolutus* Spath, p. 130, pl. 2, fig. 2; pl. 8, fig. 2; pl. 9, fig. 4, pl. 11, fig. 2.

1961. *Xenoceltites subevolutus* – Tozer, p. 53, pl. 16, fig. 1.

1978. *Xenoceltites subevolutus* – Zakharov, pl. 11, fig. 17.

1978. *Xenoceltites spitsbergensis* – Weitschat and Lehmann, p. 94, pl. 11, figs. 3b, 4, 5.

1978. *Xenoceltites subevolutus* – Weitschat and Lehmann, p. 95, pl. 11, figs. 1, 2, 3a.

1990. *Xenoceltites subevolutus* – Dagys and Ermakova, p. 23, pl. 5, fig. 4.

1994. *Xenoceltites subevolutus* – Tozer, p. 52, pl. 36, figs. 3-8.

v2013. *Xenoceltites* sp. indet. A – Brayard et al., p. 160, fig. 19a-c.

2015. *Xenoceltites subevolutus* – Piazza, p. 48, pl. 1, figs. a-c.

v2017. *Xenoceltites subevolutus* – Jattiot, p. 10, pl. 1, figs. P-AD.

2017. *Xenoceltites subevolutus* – Piazza, p. 110, fig. 4a, b.

v2018. *Xenoceltites subevolutus* – Jenks and Brayard, p. 21, fig. 21.

Occurrence: Rare in LWC46 (LWC; n = 5) and more common in LWC48 and LWC49 (LWC; n = 7). Rare in THU A1 (TR; n = 2, but two other specimens seen in the field) and common in THU A2 (TR; n = 10).

Measurements: See Fig. 5 and Table S1 (Appendix A). Estimated maximal size: ~8 cm (Jenks and Brayard, 2018).

Description: Near-serpenticonic, compressed xenoceltitid exhibiting a narrowly rounded to arched venter. Flanks slightly convex. Ornamentation highly variable among specimens and through ontogeny, generally consisting of (*i*) ventral constrictions for smooth variants, extending on flanks for robust specimens, and (*ii*) distant, low, blunt, radial to slightly prosiradiate ribs arising from the umbilical shoulder and well visible on internal whorls. Umbilicus relatively shallow with an oblique wall and rounded margin. Suture line ceratitic typical of xenoceltitids with three broad rounded saddles decreasing in size from the venter to the umbilicus. The main lateral lobe is well indented.

Remarks: *Xenoceltites subevolutus* exhibits a wide geographic distribution including USA, British Columbia (Tozer, 1994), Spitsbergen (e.g., Piazza et al., 2017), and Siberia (e.g., Dagys and Ermakova, 1990); another species attributed to the genus, *X. variocostatus*, is found in South China (Brayard and Bucher, 2008), Vietnam (Shigeta et al., 2014) and the Northern Indian Margin (Brühwiler et al., 2012a, b). Similar to other American localities such as Palomino Ridge (Jattiot et al., 2017) and Crittenden Springs (Jenks and Brayard, 2018), *Xenoceltites subevolutus* is rather rare in beds where prionitids such as *Anasibirites* occur, but become more common in overlying beds where *Pseudosageceras augustum* is present. This

species extends through much of the late Smithian. Among co-occurring American xenoceltitids, *X. subevolutus* mainly differs from *Glyptophiceras sinuatum* by somewhat weaker forward projections, and from *Condensoceras youngi* by a more evolute, serpenticonic-like coiling and by stronger ornamentation. The wide intraspecific variation of *X. subevolutus* overlaps with that of some other late Smithian xenoceltitid species, such as *G. sinuatum*, sometimes preventing firm identification. In addition, suture lines of both species are similar (compare suture lines illustrated in Fig. 4(C), the first for American specimens of *X. subevolutus*, with *G. sinuatum* material of Jattiot et al., 2017). These observations raise the still unanswered question of a possible morphological and/or evolutionary continuum among all these species.

Two specimens described as *Ophiceras matheri* and *Xenodiscus douglasensis* by Mathews (1929) from the Fort Douglas area, north-central Utah, resemble *X. subevolutus*. However, the information provided by Mathews indicates that the stratigraphic origin of these specimens is from the early Spathian "*Columbites* zone", thus preventing a firm assignment to *X. subevolutus*. A solution to resolve this conundrum is a future bed-by-bed sampling from the upper Smithian portion of the section in this area. If it yields specimens attributable to *Ophiceras matheri* and *Xenodiscus douglasensis*, then *X. subevolutus* potentially would have to be synonymized with these Mathew's (1929) taxa, given that they have priority.

Superfamily Sageceratoidea Hyatt, 1884

Family Hedenstroemiidae Waagen, 1895

Genus ***Pseudosageceras*** Diener, 1895

Type species: *Pseudosageceras* sp. indet. Diener, 1895

Pseudosageceras augustum (Brayard and Bucher, 2008)

Figs. 4(M-O), 6

?1929. *Cordillerites compressus* Mathews, p. 3, pl. 1, figs. 15-17.

?1929. *Pseudosageceras intermontanum* Hyatt and Smith, 1905 – Mathews, p. 3, pl. 1, figs. 18-21.

v2008. *Hedenstroemia augusta* Brayard and Bucher, p. 72, pl. 39, figs. 1-11, text-fig. 63.

v2010. *Pseudosageceras augustum* – Jenks et al., p.35, fig. 24.

2010b. *Pseudosageceras augustum* – Brühwiler et al., p. 429, fig. 16: 10-11.

2012b. *Pseudosageceras augustum* – Brühwiler et al., p. 171, fig. 41Z-AI.

v2017. *Pseudosageceras augustum* – Jattiot et al., p. 43, pl. 19, figs. J-N.

v2018. *Pseudosageceras augustum* – Jenks and Brayard, p. 114, fig. 104.

Occurrence: Rare in LWC48, LWC49 and LWC52 (LWC; n = 8). More common in THU A2 (TR; n = 10).

Measurements: See Fig. 7 and Table S2 (Appendix A). Estimated maximal size: ~9 cm. (Jenks and Brayard, 2018).

Description: Involute, compressed oxyconic shell. Flanks weakly convex with maximum curvature and a slight change of slope at mid-flank, producing an aspenitid-like flank contour. Some specimens appear to exhibit a longitudinal line at mid-flank. The depressed umbilical area appears nearly flat, the outer half of the flank being somewhat steeper. Venter narrowly bicarinate and tabulate on inner mold. Surface smooth excepting for sinuous, slightly biconcave and fine growth lines. Suture line ceratitic and complex, typical of the family, with numerous elongated saddles, several adventious elements and an auxiliary series.

Remarks: This species shows an intertropical, trans-Panthalassic distribution as do many other Smithian species (Brayard et al., 2009a; Jenks et al., 2010). *Pseudosageceras augustum* is very rare in localities from the Northern Indian Margin (Brühwiler et al., 2010b, 2012a) and northeastern Nevada (Jattiot et al., 2017; Jenks and Brayard, 2018). The morphology of the

American specimens is identical to the coeval type material from South China, which is relatively a little bit more abundant (Brayard and Bucher, 2008). Illustrated suture lines are often weathered and only partially preserved (Brühwiler et al., 2010b), preventing direct comparisons among specimens from distant areas. Some of the specimens described here exhibit almost the entire suture line architecture, confirming its complexity. It also shows that the main lateral lobe is trifid, justifying the assignment of this species to the genus *Pseudosageceras* as postulated by Brühwiler et al. (2010b). Lobes of the adventious series are bifid and saddles of the auxiliary series are squarer than in some other representatives of hedenstroemiids such as *Pseudosageceras multilobatum* or *Cordillerites*. ?*Pseudosageras bullatum* from Palomino Ridge, Nevada (Jattiot et al., 2017) closely resembles *P. augustum* but differs by its regularly spaced bullae located at mid-flank. A single specimen described as *Cordillerites compressus* by Mathews (1929) and two specimens he attributed to *P. intermontanum* Hyatt and Smith (1905) from the Fort Douglas area, north-central Utah, resemble *P. augustum* by their highly compressed section and narrow venter. However, he only illustrated these three specimens with limited stratigraphic information, thus preventing a firm assignment to *P. augustum*. If future bed-by-bed sampling from the upper Smithian portion of the section in this area yields specimens attributable to *C. compressus* that exhibit a characteristic widely depressed umbilical region and trifid main lateral lobe, then *P. augustum* likely would have to be synonymized with Mathew's (1929) taxon, given that it has priority.

Based on ammonoid occurrences in the Tulong section (South Tibet), *P. augustum* may have survived the SSB up to the early Spathian *Procolumbites* beds (Brühwiler et al., 2010b), but no illustrations and firm occurrence reports of these Spathian specimens have been provided so far. Until new discoveries are made, it is therefore preferable to consider this species as characteristic only of the latest Smithian.

Superfamily Meekoceratoidea Waagen, 1895

Family Prionitidae Waagen, 1895

Genus ***Gurleyites*** Mathews, 1929

Type species: *Gurleyites smithi* Mathews, 1929

Remarks: Brayard et al. (2020) provided a comprehensive revision and review of the taxonomy of *Gurleyites smithi*, previously assigned to the doubtful genus *Arctoprionites*. We follow the conclusions of this work and thus do not include the complete description for this species.

Gurleyites smithi Mathews, 1929

Figs. 8, 9(A-I)

v2020. *Gurleyites smithi* – Brayard et al., figs. 7-8, 9A-J, 10 [cum syn.].

Occurrence: Abundant in LWC45, LWC46 (LWC; n = 45) and rare in THU A1 (TR; n = 2).

Measurements: See Fig. 10 and Table S3 (Appendix A). Estimated maximal size: ~15 cm (Jenks and Brayard, 2018).

Description: Compressed and moderately involute prionitid showing a slightly egressive coiling, and a marked intraspecific variation among specimens and throughout ontogeny. Ornamentation typically consists of forward projected, bullate, elongated and sinuous ribs that stem near the umbilical shoulder and fade rapidly toward the venter. Ribs may cross the venter forming a slightly crenulated venter. Strigation may also be visible on the venter and on the ventrolateral margins of well-preserved specimens, as already discussed in Brayard et al. (2020). In some cases, elevated bullate ribs almost form tubercles. Umbilical margin is broadly arched with an inclined wall. The suture line exhibits three large, arched saddles, decreasing in size from the ventrolateral to the umbilical margin. Lobes are well indented.

Remarks: This species shows a marked intraspecific variation that overlaps with other highly variable species belonging to several prionitid genera, such as *Wasatchites* and *Anasibirites*, but more specifically with *Hemiprionites typus*, thus making some specimen assignments difficult (see Brayard et al., 2020 for a discussion on this point). Six specimens sampled at LWC also show a specificity that had rarely been noticed before. These specimens are indeed clearly more evolute at identical sizes than the others (Figs. 9(A-D), 10). Rare specimens with a similar coiling have already been illustrated in Jenks and Brayard (2018: e.g., fig. 87A-C). This feature generally concerns specimens having a diameter greater than 50 mm. All have the typical and variable ornamentation of *G. smithi*, as well as an identical suture line, supporting their assignment to *G. smithi*. These extreme morphologies highlight the wide intraspecific variation of this taxon.

As with many other prionitids, *Gurleyites smithi* shows a rather cosmopolitan distribution (Spitsbergen: Frebold, 1930, Piazza et al., 2017; British Columbia: Tozer, 1994) but is often relatively rare. This species has been found at several places in the western USA basin (Brayard et al., 2013; Jattiot et al., 2017, 2018; Jenks and Brayard, 2018), but it has been abundantly sampled only in southwestern-most Utah up to now (Brayard et al., 2020). LWC is a new site where *G. smithi* is relatively rather abundant.

Genus ***Wasatchites*** Mathews, 1929

Type species: *Wasatchites perrini* Mathews, 1929

Remarks: The reader is referred to Brayard et al. (2013) for a thorough discussion of the typical early late Smithian genus *Wasatchites*. Brayard et al. (2013), Jattiot et al. (2017) and Jenks and Brayard (2018) provided the most recent detailed descriptions and discussions of *W. perrini*. Based on the conclusions of these works, we thus only include below a simplified description for this species.

Wasatchites perrini Mathews, 1929

Fig. 11

v2020. *Wasatchites perrini* – Brayard et al., fig. 9K-L [cum syn.].

Occurrence: Common in LWC45, LWC46 (LWC; n = 22). Not found in THU A1 (TR).

Measurements: see Fig. 12 and Table S4 (Appendix A). Estimated maximal size: ~20 cm (Jenks and Brayard, 2018).

Description: Coiling generally moderately involute. Trapezoidal whorl section. Ornamentation typical and showing (*i*) very conspicuous tubercles on umbilical shoulders that become more bullate or nodate on mature whorls, but then tend to rapidly lose strength near the aperture, and (*ii*) alternating strong and weak, fasciculate ribs that stem from the tubercles and cross the venter. The venter is subtabulate to slightly arched. Suture line typical of prionitids with three rounded saddles, decreasing in size toward the umbilicus, and a deep first lateral lobe.

Remarks: *W. perrini* can be distinguished from other co-occurring taxa by its conspicuous, regularly spaced ornamentation. It also differs from *W.* cf. *distractus* by its more tabulate-to-arched venter and the more umbilicate position of its tubercles, and fasciculate ribs.

Genus ***Anasibirites*** Mojsisovics, 1896

Type species: *Sibirites kingianus* Waagen, 1895

Remarks: Reader should refer to Jattiot et al. (2016) for a comprehensive review of the taxonomy of the various *Anasibirites* species and associated diagnostic characters, as well as Jattiot et al. (2016) and Brayard et al. (2020) for complete synonymy lists.

Anasibirites cf. *kingianus* (Waagen, 1895)

Fig. 9(J-N)

v2016. *Anasibirites kingianus* – Jattiot et al., p. 183, figs. 4, 6-9, 10A–M, 12, 15–18 [cum syn.].

v2017. *Anasibirites kingianus* – Jattiot and Bucher in Jattiot et al., p. 29, pl. 11, figs. A–F.

2017. *Anasibirites kingianus* – Piazza in Piazza et al., fig. 4F-I.

v2018. *Anasibirites kingianus* – Jenks and Brayard, p. 73, fig. 74A–C.

Occurrence: Very rare in LWC45, LWC46 (LWC; n = 5). Not found in THU A1 (TR).

Measurements: See Fig. 13 and Table S5 (Appendix A). Estimated maximal size: ~10 cm (Jattiot et al., 2016).

Description: Prionitid with a rather involute coiling. Coiling is more evolute and whorl section is generally quadrate for small-sized (<20 mm) specimens, but becomes more involute and compressed for larger specimens. Venter varies from tabulate to arched. Ornamentation on inner whorls typically consists of megastriae, variable in strength, and becoming denser and weaker during ontogeny. Ribs are also visible on some specimens. Suture line not visible on our specimens.

Remarks: *A. kingianus* is one of the most abundant late Smithian taxon worldwide outside the western USA basin. *A. kingianus* is rare in this area (Mathews, 1929; Jattiot et al., 2016; Jenks and Brayard, 2018), where the late Smithian prionitid fauna is often dominated by *A. multiformis* (Brayard et al., 2013, 2020). In accordance with this observation, *A.* cf. *kingianus* is rare in LWC and was not found in TR. The reader is referred to Jattiot et al. (2016) for a thorough morphological comparison between the two co-occurring species *A. kingianus* and *A. multiformis*, and for a discussion on their respective cosmopolitan distribution. As it is difficult to distinguish both *Anasibirites* species based on small and imperfectly preserved specimens (Jattiot et al., 2016; Jenks and Brayard, 2018), the determination of specimens

belonging to *A. kingianus* was mainly based on the presence of irregular, marked megastriae disappearing during ontogenesis. Thus, attribution of these five specimens can be questioned.

Anasibirites multiformis Welter, 1922

Fig. 14

v2016. *Anasibirites multiformis* – Jattiot et al., p. 184, figs. 10N–S, 21–23 [cum syn.].

v2017. *Anasibirites multiformis* – Jattiot and Bucher in Jattiot et al., p. 30, pl. 11, figs. G-AA.

v2018. *Anasibirites multiformis* – Jenks and Brayard, p. 79, figs. 74D-F, G(4,5), 75.

v2020. *Anasibirites multiformis* – Brayard et al., fig. 11.

Occurrence: Abundant in LWC45, LWC46 (LWC; n = 80) and THU A1 (TR; n = 6).

Measurements: See Fig. 15 and Table S6 (Appendix A). Estimated maximal size: ~10 cm (Jattiot et al., 2016).

Description: Simplified description from Brayard et al. (2020): rather involute, compressed prionitid with near isometric growth. Ornamentation typically consists of weak and dense megastriae throughout ontogeny. Suture line ceratitic with deep and well indented lobes. Broad saddles are gently bend toward umbilicus, especially on larger specimens (Fig. 14(R)).

Remarks: see above, discussion of *A.* cf. *kingianus*.

Genus ***Hemiprionites*** Spath, 1929

Type species: *Goniodiscus typus* Waagen, 1895

Hemiprionites typus (Waagen, 1895)

Figs. 9(C), 16, 17(A-K)

1895. *Goniodiscus typus* Waagen, p. 128, pl. 9, figs. 7-10.

1929. *Goniodiscus typus* – Mathews, p. 31, pl. 5, figs. 12-21.

1929. *Goniodiscus americanus* – Mathews, p. 32, pl. 5, figs. 22-27.

1929. *Goniodiscus shumardi* – Mathews, p. 33, pl. 6, figs. 11-14.

1929. *Goniodiscus utahensis* – Mathews, p. 33, pl. 6, figs. 29-31.

1929. *Goniodiscus slocomi* – Mathews, p. 34, pl. 6, figs. 15-17.

1929. *Goniodiscus butleri* – Mathews, p. 35, pl. 6, figs. 18-21.

1932. *Anasibirites typus* – Smith, p. 76, pl. 80, figs. 6-8.

1932. *Anasibirites utahensis* – Smith, p. 77, pl. 80, figs. 9, 10.

1934. *Hemiprionites typus* – Spath, p. 331, figs. 114ac.

vp2008. *Hemiprionites* cf. *H. butleri* – Brayard and Bucher, p. 58, pl. 29, figs. 1, 4, 7 only, text- fig. 50.

2012b. *Hemiprionites typus* – Brühwiler and Bucher, p. 103, figs. 89A-AH.

v2013. *Hemiprionites* cf. *H. typus* – Brayard et al., p. 197, fig. 66.

v2017. *Hemiprionites typus* – Jattiot and Bucher in Jattiot et al., p. 31, pl. 12, figs. A-M, pl. 13, figs. A-X.

vp2018. *Hemiprionites typus* – Jenks and Brayard, p. 81, figs. 77, 78A-C, 78G-R, 79A-F,.79J-O.

v2020. *Hemiprionites typus* – Brayard et al., fig. 12J-S.

2020. *Hemiprionites typus* – Jattiot et al., p. 56, pl. 29, figs. U-AL.

Occurrence: Abundant in LWC45, LWC46 (LWC; n = 74) and rare in THU A1 (TR; n = 3).

Measurements: See Fig. 18 and Table S7 (Appendix A). Estimated maximal size: ~10 cm (Jattiot et al., 2017).

Description: Main diagnostic characteristics of *Hemiprionites* species have recently been reviewed by Jattiot et al. (2017). We only repeat here the simplified description recently given by Brayard et al. (2020): “compressed shell with variable involution and a typical marked egressive coiling at mature stage. A small depression on the outer edge of the flank, just

below the ventral margin, is also visible on some specimens. Spiral lines are sometimes visible on the venter and/or near the ventrolateral margin. Flexuous and slightly biconcave growth lines are visible and may bundle into small folds that may cross the venter. Suture line ceratitic with a deep and flared first lateral lobe. Saddles appear pinched". One specimen from LWC46 (Fig. 16(J, K)) exhibits umbilical saddles that are slightly bent toward umbilicus and somewhat flattened on their ventral side. This feature may be included in the rather large intraspecific variation of the suture line known for *H. typus* (Jattiot et al., 2017, 2020; Jenks and Brayard, 2018).

Remarks: *H. typus* can be distinguished from the co-occurring *H. walcotti*, by its often wider venter and more evolute and egressive coiling. Some specimens of *H. typus* also exhibit a small depression near the ventral margin. As discussed by Brayard et al. (2020), the morphological variability of *H. typus* partly overlaps with that of *Gurleyites smithi*, but the latter appears more ornamented and slightly more evolute. Its saddles are also generally more broadly rounded.

Hemiprionites walcotti (Mathews, 1929)

Fig. 17(L-R)

p1922. *Anasibirites multiformis* Welter, p. 17, figs. 4-7, 11-14.

1929. *Goniodiscus walcotti* Mathews, p. 32, pl. 6, figs. 1-5.

1934. *Hemiprionites timorensis* Spath, p. 331.

vp2008. *Hemiprionites* cf. *H. butleri* – Brayard and Bucher, p. 58, pl. 29, figs. 2, 3, 6 only.

v2008. *Hemiprionites klugi* Brayard and Bucher, p. 59, pl. 30, figs. 1-4.

p2012a. *Hemiprionites* cf. *H. butleri* – Brühwiler and Bucher, p. 33, pl. 19, figs. 10 only.

p2012b. *Anasibirites angulosus* – Brühwiler and Bucher, p. 103, figs. 87H-J, N-P only.

2012b. *Hemiprionites klugi* – Brühwiler and Bucher, p. 103, figs. 87Q-AB.

v2017. *Hemiprionites walcotti* – Jattiot and Bucher in Jattiot et al., p. 34, pl. 14, figs. A-Y.

v2018. *Hemiprionites walcotti* – Jenks and Brayard, p. 83, figs. 79Q-V.

v2020. *Hemiprionites walcotti* – Brayard et al., fig. 12A-I.

2020. *Hemiprionites walcotti* – Jattiot et al., p. 57, pl. 29, figs. AO-BG.

Occurrence: Proportionally rare in LWC45, LWC46 (LWC; n = 8) and more common in THU A1 (TR; n = 4).

Measurements: See Fig. 19 and Table S8 (Appendix A). Estimated maximal size: ~7 cm (Jattiot et al., 2017).

Description: See the taxonomic revision of *Hemiprionites* species by Jattiot et al. (2017).

Remarks: See *H. typus* discussion.

4. Discussion

4.1. Late Smithian ammonoid biostratigraphy in the western USA Basin

At both LWC and TR, two distinct, successive late Smithian assemblages were sampled. The lowest corresponds to the *Anasibirites multiformis* beds found elsewhere in the western USA basin (UAZ5 of Jattiot et al., 2017). It contains the cosmopolitan prionitid taxa typical of the first part of the late Smithian, such as *Anasibirites*, *Wasatchites*, *Gurleyites* and *Hemiprionites*. Some rare specimens of *Xenoceltites subevolutus* also co-occur, similarly to other sites in Nevada (Jattiot et al., 2017; Jenks and Brayard, 2018). This assemblage is thus correlative of the *Anasibirites* and *Wasatchites* beds found worldwide (e.g., Jenks et al., 2015). *Xenoceltites subevolutus* and *Pseudosageceras augustum* are the only two species that co-occur in the overlying assemblage. Although species-poor compared to coeval assemblages from Nevada, where some other hedenstroemiids (e.g., ?*Pseudosageceras bullatum*) and xenoceltitids (e.g., *Glyptophiceras sinuatum*) taxa can also be present (Jattiot et al., 2017; Jenks and Brayard, 2018), this association is typical of the second part of the late

539 Smithian in Nevada and worldwide. It thus validates the existence of a regional zone
540 representing this interval outside Nevada (postulated UAZ6 of Jattiot et al., 2017) in the
541 western USA basin. This zone also therefore correlates with the latest Smithian UAZ S-14
542 recognized from southern Tethyan basins (*G. sinuatum* beds; Brühwiler et al., 2011). It
543 consequently significantly expands possible correlation between these very distant areas and
544 thus enhance inter-basin comparisons during this crucial time interval. Additionally, these
545 new data corroborate other occurrences of *Xenoceltites subevolutus* throughout most of the
546 late Smithian (Brühwiler et al., 2011; Jattiot et al., 2017; Jenks and Brayard, 2018).
547
548 *4.2. The biogeography of middle and late Smithian American ammonoids*
549 As a preliminary attempt to synthesize and compare the available middle to late
550 Smithian ammonoid records through time and space, we compiled the published generic
551 occurrences for three major, well-documented and distant areas: the Panthalassic western
552 USA basin (data from Brayard et al., 2009a, 2013, 2020; Jenks et al., 2010; Jattiot et al., 2016,
553 2017; Jenks and Brayard, 2018) and South China (data from Brayard and Bucher, 2008) and
554 the Tethyan Northern Indian Margin (data from Brühwiler et al., 2012a, b) (Fig. 20). Among
555 the 79 genera recorded in these three areas, 71 occur in the middle Smithian and 11 in the late
556 Smithian, including only three genera crossing the middle/late Smithian boundary
557 (*Hemiprionites*, *Pseudosageceras* and *Subvishnuites*).
558 Among the 71 middle Smithian genera, 40 of them (56%) appear endemic to one of
559 the three areas, 13 in the western USA basin, 16 in the Northern Indian Margin, and 10 in
560 South China. Conversely, 13 genera co-occur in the western USA basin and South China,
561 whereas the Northern Indian Margin basin shares only 4 and 3 genera with South China and
562 the western USA basin, respectively. The 12 remaining genera are found in the three areas. A
563 total of 41 middle Smithian genera are found in the western USA basin, among which five of

them are from a single locality – Crittenden Springs (Jenks and Brayard, 2018). Excluding these endemic taxa, 75% of the western USA middle Smithian ammonoid genera are therefore found in at least one of the two other compared areas, which highlights a well-established trans-Panthalassic circulation of ammonoids at that time (Brayard et al., 2007, 2009a, 2009b; Jenks et al., 2010; Shigeta and Kumagae, 2015; Jenks and Brayard, 2018). They are also often long-ranging with temporal distributions extending throughout the middle Smithian (Jattiot et al., 2017).

Departing from this highly diversified and well contrasted middle Smithian biogeographical configuration, the late Smithian assemblages include 11 genera among which 8 are known from western USA localities, 9 occur in the Northern Indian Margin, and 6 in South China. Out of these 11 genera, 4 are restricted to one of the three compared areas, whereas 2 are found in two areas, and 5 occur in the three areas, pointing toward a late Smithian ammonoid distribution significantly more cosmopolitan than during the middle Smithian (one-tailed Fisher's exact test: $p = 0.038$*). Based on the three compared areas, the global extinction event occurring at the middle/late Smithian boundary and further impacting late Smithian assemblages worldwide once again appears as a time of significant biogeographical homogenization. This event echoes the effect of the Permian/Triassic mass extinction on ammonoid biogeographic distribution, as already discussed in previous works (Brayard et al., 2006, 2007, 2009b, 2013, 2015; Jattiot et al., 2016, 2018; Dai and Song, 2020). A possible exception to this global homogenization pattern is represented by the unusual late Smithian ammonoid assemblages reported from South Primorye (Zakharov et al., 2013, in press). However, the local ammonoid occurrences and correlations between this region and other worldwide localities must be further deciphered to determine its exact significance in understanding late Smithian events and in the survival and evolution of ammonoids through the SSB.

589

590 *4.3. Extending the late Smithian ammonoid record – a conclusive remark*

591 With respect to the western USA ammonoid record, the new occurrences of the late
592 Smithian UAZ6 outside Nevada as described in this work suggest that this typical ammonoid
593 assemblage can likely be found more broadly within the western USA basin. This time
594 interval corresponds to a marine regression at a global scale (e.g., Widmann et al., 2020), but
595 to a transgression in the northern part of the western USA basin (Caravaca et al., 2018;
596 Brayard et al., 2020). Potential fossiliferous localities are therefore most likely to be found in
597 a reduced number within the basin and preferentially in places where regional subsidence is
598 able to compensate for the global regression. Such localities are likely scarce in the southern
599 part of the basin where the sea had already receded by that time (Lucas et al., 2007; Olivier et
600 al., 2018; Brayard et al., 2020), but are more likely present in the western and northern parts
601 of the basin where local subsidence was potentially able to compensate for this regression
602 (Caravaca et al., 2018). However, deposits corresponding to UAZ6 often form incompetent
603 hills, where outcrops are rare and hardly discernible in the landscape, and where the high
604 proportion of shales does not facilitate a high quality of preservation in these localities. The
605 same observations probably apply to the new, potentially latest Smithian ammonoid
606 assemblage reported from northeastern Nevada by Widmann et al. (2020), and it is likely that
607 its record elsewhere will be very sparse. A detailed knowledge of this potential latest Smithian
608 ammonoid zone will likely be crucial in understanding the evolutionary history of ammonoids
609 through the SSB and postulate refined phylogenetic links between late Smithian and early
610 Spathian ammonoids.

611

612 **Acknowledgements**

This work is a contribution to the ANR project AFTER (ANR-13-JS06-0001-01) and was also supported by the French “Investissements d’Avenir” program, project ISITE-BFC (ANR-15-IDEX-03). The final version of this paper benefited from constructive reviews by Marco Balini and Yuri Zakharov. We thank G. Caravaca and A.-S. Grosjean for their help in the field, and private land owners (Scott Rees – south side of Weber River and Mrs. Monte Brough – north side of Weber River) for allowing access to their lands. The Thumb Ridge section is located on US public land under the stewardship of the Bureau of Land Management (BLM) of the US Department of the Interior; access to these lands is gratefully acknowledged.

References

Baresel, B., Bucher, H., Brosse, M., Cordey, F., Guodun, K., Schaltegger, U., 2017. Precise age for the Permian–Triassic boundary in South China from high-precision U-Pb geochronology and Bayesian age–depth modeling. Solid Earth 8, 361-378.

Brayard, A., Brühwiler, T., Bucher, H., Jenks, J., 2009a. *Guodunites*, a low-palaeolatitude and trans-Panthalassic Smithian (Early Triassic) ammonoid genus. Palaeontology 52, 471-481.

Brayard, A., Bucher, H., 2008. Smithian (Early Triassic) ammonoid faunas from northwestern Guangxi (South China): taxonomy and biochronology. Fossils and Strata 55, 1-179.

Brayard, A., Bucher, H., 2015. Permian-Triassic extinctions and rediversifications. In: C. Klug et al. (Eds), Ammonoid Paleobiology: From macroevolution to paleogeography. Topics in Geobiology 44, Springer Netherlands, pp. 465-473.

Brayard, A., Bucher, H., Escarguel, G., Fluteau, F., Bourquin, S., Galfetti, T., 2006. The Early Triassic ammonoid recovery: paleoclimatic significance of diversity gradients. Palaeogeography, Palaeoclimatology, Palaeoecology 239, 374-395.

637 Brayard, A., Bylund, K., Jenks, J., Stephen, D., Olivier, N., Escarguel, G., Fara, E., Vennin,
638 E., 2013. Smithian ammonoid faunas from Utah: implications for Early Triassic
639 biostratigraphy, correlation and basinal paleogeography. Swiss Journal of Palaeontology
640 132, 141-219.
641 Brayard, A., Escarguel, G., Bucher, H., 2007. The biogeography of Early Triassic ammonoid
642 faunas: Clusters, gradients and networks. Geobios 40, 749-765.
643 Brayard, A., Escarguel, G., Bucher, H., Brühwiler, T., 2009b. Smithian and Spathian (Early
644 Triassic) ammonoid assemblages from terranes: Paleoceanographic and paleogeographic
645 implications. Journal of Asian Earth Sciences 36, 420-433.
646 Brayard, A., Jenks, J.F., Bylund, K.G., the Paris Biota team, 2019. Ammonoids and nautiloids
647 from the earliest Spathian Paris Biota and other early Spathian localities in southeastern
648 Idaho, USA. Geobios 54, 13-36.
649 Brayard, A., Olivier, N., Vennin, E., Jenks, J., Bylund, K., Stephen, D., McShinsky, D.,
650 Goudemand, N., Fara, E., Escarguel, G., 2020. New middle and late Smithian ammonoid
651 faunas from the Utah/Arizona border: new evidence for calibrating Early Triassic
652 transgressive-regressive trends and paleobiogeographical signals in the western USA basin.
653 Global and Planetary Change 192, 103251.
654 Brosse, M., Brayard, A., Fara, E., Neige, P., 2013. Ammonoid recovery after the Permian–
655 Triassic mass extinction: a re-exploration of morphological and phylogenetic diversity
656 patterns. Journal of the Geological Society 170, 225-236.
657 Brühwiler, T., Bucher, H., Brayard, A., Goudemand, N., 2010a. High-resolution
658 biochronology and diversity dynamics of the Early Triassic ammonoid recovery: The
659 Smithian faunas of the Northern Indian Margin. Palaeogeography, Palaeoclimatology,
660 Palaeoecology 297, 491-501.

Brühwiler, T., Bucher, H., Goudemand, N., 2010b. Smithian (Early Triassic) ammonoids from Tulong, South Tibet. Geobios 43, 403-431.

Brühwiler, T., Bucher, H., Roohi, G., Yaseen, A., Rehman, K., 2011. A new early Smithian ammonoid fauna from the Salt Range (Pakistan). Swiss Journal of Palaeontology 130, 187-201.

Brühwiler, T., Bucher, H., Krystyn, L., 2012a. Middle and late Smithian (Early Triassic) ammonoids from Spiti (India). Special Papers in Palaeontology 88, 115-174.

Brühwiler, T., Bucher, H., Ware, D., Hermann, E., Hochuli, P.A., Roohi, G., Rehman, K., Yassen, A., 2012b. Smithian (Early Triassic) ammonoids from the Salt Range. Special Papers in Palaeontology 88, 1-114.

Caravaca, G., Brayard, A., Vennin, E., Guiraud, M., Le Pourhiet, L., Grosjean, A.-S., Thomazo, C., Olivier, N., Fara, E., Escarguel, G., Bylund, K.G., Jenks, J.F., Stephen, D.A., 2018. Controlling factors for differential subsidence in the Sonoma Foreland Basin (Early Triassic, western USA). Geological Magazine 155, 1305-1329.

Clark, D.L., Oviatt, C.G., 2019. Interim geologic map of the Bonneville Salt Flats and east part of the Wendover 30' X 60' Quadrangles, Tooele County, Utah, East Part — Year 2. Utah Geological Survey, Open-File Report 702.

Dai, X., Song, H., 2020. Toward an understanding of cosmopolitanism in deep time: a case study of ammonoids from the middle Permian to the Middle Triassic. Paleobiology 46, 533-549.

Dagys, A.S., 1988. Major features of the geographic differentiation of Triassic ammonoids. In: Wiedmann, J., Kullmann, J. (Eds.), Cephalopods - Present and past. Schweizerbart'sche Verlagsbuchhandlung, Stuttgart, pp. 341-349.

Dagys, A.S., Ermakova, S.P., 1990. Early Olenekian ammonoids of Siberia. Nauka, Moskow.

685 Doelling, H.H., Solomon, K.J., Davies, S.F., 1994. Geologic map of the Grayback Hills
686 Quadrangle, Tooele Co., Utah. Utah Geological Survey Map 166.
687 Donovan, R.C. 1986. Taphonomy of the *Meekoceras* beds, Thaynes Formation (Lower
688 Triassic), Idaho, Utah and Nevada. Ms. Thesis, University of Wyoming, 98 p.
689 Ermakova, S.P., 2002. Zonal standard of the Boreal Lower Triassic. Nauka, Moscow.
690 Frebold, H., 1930. Die altersstellung des fischhorizontes, des grippianiveaus und des unteren
691 saurierhorizontes in Spitzbergen. Skrifter om Svalbard og Ishavet 28, 1-36.
692 Galfetti, T., Bucher, H., Martini, R., Hochuli, P.A., Weissert, H., Crasquin-Soleau, S.,
693 Brayard, A., Goudemand, N., Brühwiler, T., Guodun, K., 2008. Evolution of Early Triassic
694 outer platform paleoenvironments in the Nanpanjiang Basin (South China) and their
695 significance for the biotic recovery. Sedimentary Geology 204, 36-60.
696 Galfetti, T., Bucher, H., Ovtcharova, M., Schaltegger, U., Brayard, A., Brühwiler, T.,
697 Goudemand, N., Weissert, H., Hochuli, P.A., Cordey, F., Guodun, K.A., 2007. Timing of
698 the Early Triassic carbon cycle perturbations inferred from new U-Pb ages and ammonoid
699 biochronozones. Earth and Planetary Science Letters 258, 593-604.
700 Goudemand, N., Romano, C., Leu, M., Bucher, H., Trotter, J.A., Williams, I.S., 2019.
701 Dynamic interplay between climate and marine biodiversity upheavals during the early
702 Triassic Smithian-Spathian biotic crisis. Earth-Science Reviews 195, 169-178.
703 Grasby, S.E., Beauchamp, B., Embry, A., Sanei, H., 2013. Recurrent Early Triassic ocean
704 anoxia. Geology 41, 175-178.
705 Grosjean, A.-S., Vennin, E., Olivier, N., Caravaca, G., Thomazo, C., Fara, E., Escarguel, G.,
706 Bylund, K.G., Jenks, J.F., Stephen, D.A., Brayard, A., 2018. Early Triassic environmental
707 dynamics and microbial development during the Smithian–Spathian transition (Lower
708 Weber Canyon, Utah, USA). Sedimentary Geology 363, 136-151.

709 Hermann, E., Hochuli, P.A., Bucher, H., Brühwiler, T., Hautmann, M., Ware, D., Weissert,
710 H., Roohi, G., Yaseen, A., Khalil-ur-Rehman, 2012. Climatic oscillations at the onset of
711 the Mesozoic inferred from palynological records from the North Indian Margin. Journal
712 of the Geological Society 169, 227-237.
713 Jattiot, R., Brayard, A., Bucher, H., Vennin, E., Caravaca, G., Jenks, J.F., Bylund, K.G.,
714 Escarguel, G., 2018. Palaeobiogeographical distribution of Smithian (Early Triassic)
715 ammonoid faunas within the western USA basin and its controlling parameters.
716 Palaeontology 61, 881-904.
717 Jattiot, R., Bucher, H., Brayard, A., Brosse, M., Jenks, J. F., Bylund, K.G., 2017. Smithian
718 ammonoid faunas from northeastern Nevada: implications for Early Triassic
719 biostratigraphy and correlation within the western USA basin. Palaeontographica
720 Abteilung A 309, 1-89.
721 Jattiot, R., Bucher, H., Brayard, A., Monnet, C., Jenks, J.F., Hautmann, M., 2016. Revision of
722 the genus *Anasibirites* Mojsisovics (Ammonoidea): an iconic and cosmopolitan taxon of
723 the late Smithian (Early Triassic) extinction. Papers in Palaeontology 2, 155-188.
724 Jattiot, R., Bucher, H., Brayard, A., 2020. Smithian (Early Triassic) ammonoid faunas from
725 Timor: taxonomy and biochronology. Palaeontographica A 317, 1-137.
726 Jenks, J., Brayard, A., 2018. Smithian (Early Triassic) ammonoids from Crittenden Springs,
727 Elko County, Nevada: Taxonomy, biostratigraphy and biogeography. New Mexico
728 Museum of Natural History and Science, Bulletin 78, 1-175.
729 Jenks, J., Brayard, A., Brühwiler, T., Bucher, H., 2010. New Smithian (Early Triassic)
730 ammonoids from Crittenden Springs, Elko County, Nevada: Implications for taxonomy,
731 biostratigraphy and biogeography. New Mexico Museum of Natural History and Science,
732 Bulletin 48, 1-41.

733 Jenks, J.F., Monnet, C., Balini, M., Brayard, A., Meier, M., 2015. Biostratigraphy of Triassic
734 ammonoids. In: C. Kluget al. (Eds). Ammonoid Paleobiology: From macroevolution to
735 paleogeography. Topics in Geobiology 44, Springer Netherlands, pp. 329-388.
736 Kummel, B., 1954. Triassic stratigraphy of Southeastern Idaho and adjacent areas. USGS
737 Professional Paper 254-H, 1-194.
738 Kummel, B., 1957. Paleoecology of Lower Triassic formations of southeastern Idaho and
739 adjacent areas. Geological Society of America Memoir 67, 437-468.
740 Lucas, S.G., Krainer, K., Milner, A.R., 2007. The type section and age of the Timpoweap
741 Member and stratigraphic nomenclature of the Triassic Moenkopi Group in Southwestern
742 Utah. New Mexico Museum of Natural History and Science Bulletin 40, 109-117.
743 Mathews, A.A.L., 1929. The Lower Triassic cephalopod fauna of the Fort Douglas area, Utah.
744 Walker Museum Memoirs 1, 1-46.
745 Mullens, T.E., Laraway, W.H., 1964. Geology of the Devils Slide Quadrangle, Morgan and
746 Summit Counties, Utah. USGS Mineral Investigations Field Studies Map MF-290.
747 Olivier, N., Fara, E., Vennin, E., Bylund, K.G., Jenks, J.F., Escarguel, G., Stephen, D.A.,
748 Goudemand, N., Snyder, D., Thomazo, C., Brayard, A., 2018. Late Smithian microbial
749 deposits and their lateral marine fossiliferous limestones (Early Triassic, Hurricane Cliffs,
750 Utah, USA). Facies 64, 13.
751 Orchard, M.J., 2007. Conodont diversity and evolution through the latest Permian and Early
752 Triassic upheavals. Palaeogeography, Palaeoclimatology, Palaeoecology 252, 93-117.
753 Payne, J.L., Lehrmann, D.J., Wei, J., Orchard, M.J., Schrag, D.P., Knoll, A.H., 2004. Large
754 perturbations of the carbon cycle during recovery from the end-Permian extinction.
755 Science 305, 506-509.

Piazza, V., Hammer, Ø., Jattiot, R., 2017. New late Smithian (Early Triassic) ammonoids from the Lusitandiadalan Member, Vikinghøgda Formation, Svalbard. Norwegian Journal of Geology 97, 105-117.

Romano, C., Goudemand, N., Vennemann, T.W., Ware, D., Schneebeli-Hermann, E., Hochuli, P.A., Brühwiler, T., Brinkmann, W., Bucher, H., 2013. Climatic and biotic upheavals following the end-Permian mass extinction. Nature Geoscience 6, 57-60.

Schick, R.B, 1955. Geology of the Morgan-Henefer area, Utah. University of Utah, Ms. Thesis, 54 p.

Shigeta, Y., Komastu, T., Maekawa, T., Dang, H.T., 2014. Olenekian (Early Triassic) stratigraphy and fossil assemblages in northeastern Vietnam. National Museum of Nature and Science Monographs, Tokyo.

Shigeta, Y., Kumagae, T., 2015. *Churkites*, a Trans-Panthalassic Early Triassic ammonoid genus from South Primorye, Russian Far East. Paleontological Research 19, 219-236.

Smith, J.P., 1932. Lower Triassic ammonoids of North America. USGS Professional Paper 167, 1-199.

Smith, H.P., 1969. The Thaynes Formation of the Moenkopi Group North-Central Utah. Ph.D. dissertation, University of Utah (unpubl.).

Smyshlyaeva, O.P., Zakharov, Y., Popov, A.M., Bondarenko, L.G., Borisov, I.V., 2018. Stratigraphic subdivisions of the Lower Triassic of South Primorye region. Article 3. First findings of *Euflemingites prynadai* and *Shimanskyites shimanskyi* (Ammonoidea) in the SMID Section. Russian Journal of Pacific Geology 12, 469-486.

Spath, L.F., 1934. Part 4: The Ammonoidea of the Trias, Catalogue of the fossil Cephalopoda in the British Museum (Natural History). The Trustees of the British Museum, London.

Thomazo, C., Brayard, A., Elmeknassi, S., Vennin, E., Olivier, N., Caravaca, G., Escarguel, G., Fara, E., Bylund, K.G., Jenks, J.F., Stephen, D.A., Killingsworth, B., Sansjofre, P.,

781 Cartigny, P., 2019. Multiple sulfur isotope signals associated with the late Smithian event
782 and the Smithian/Spathian boundary. Earth-Science Reviews 195, 96-113.
783 Tozer, E.T., 1981. Triassic Ammonoidea: classification, evolution and relationship with
784 Permian and Jurassic forms. In: House, M.R., Senior, J.R. (Eds.), The Ammonoidea. The
785 Systematics association, London, pp. 65-100.
786 Tozer, E.T., 1982. Marine Triassic faunas of North America: their significance for assessing
787 plate and terrane movements. Geologische Rundschau 71, 1077-1104.
788 Tozer, E.T., 1994. Canadian Triassic ammonoid faunas. Geologic Survey of Canada Bulletin
789 467, 1-663.
790 Vennin, E., Olivier, N., Brayard, A., Bour, I., Thomazo, C., Escarguel, G., Fara, E., Bylund,
791 K.G., Jenks, J.F., Stephen, D.A., Hofmann, R., 2015. Microbial deposits in the aftermath of
792 the end-Permian mass extinction: A diverging case from the Mineral Mountains (Utah,
793 USA). Sedimentology 62, 753-792.
794 Widmann, P., Bucher, H., Leu, M., Vennemann, T., Bagherpour, B., Schneebeli-Hermann, E.,
795 Goudemand, N., Schaltegger, U., 2020. Dynamics of the largest carbon isotope excursion
796 during the Early Triassic biotic recovery. Frontiers in Earth Science 8, 196.
797 Yurchyk, S.L., 2011. Interpreting Early Triassic (Smithian) sea-level change and climate
798 using sequence stratigraphy and oxygen isotopes of conodont apatite. M.Sc. Thesis,
799 University of Mexico (unpubl.).
800 Zakharov, Y.D., Bondarenko, L.G., Popov, A.M., Smyshlyaeva O.P., in press. New findings
801 of latest Early Olenekian (Early Triassic) fossils in South Primorye, Russian Far East, and
802 their stratigraphical significance: Journal of Earth Science.
803 Zakharov, Y.D., Bondarenko, L.G., Smyshlyaeva, O.P., Popov, A.M., 2013. Late Smithian
804 (Early Triassic) ammonoids from *Anasibirites nevolini* Zone of South Primorye, Russian
805 Far East. New Mexico Museum of Natural History and Science Bulletin 61, 597-622.

Zhang, F., Romaniello, S.J., Algeo, T.J., Lau, K.V., Clapham, M.E., Richoz, S., Herrmann, A.D., Smith, H., Horacek, M., Anbar, A.D., 2018. Multiple episodes of extensive marine anoxia linked to global warming and continental weathering following the latest Permian mass extinction. Science Advances 4, e1602921.

Zhang, L., Orchard, M.J., Brayard, A., Algeo, T.J., Zhao, L., Chen, Z.-Q., Lyu, Z., 2019. The Smithian/Spathian boundary (late Early Triassic): A review of ammonoid, conodont, and carbon-isotopic criteria. Earth-Science Reviews 195, 7-36.

Zhao, H., Algeo, T.J., Liu, Y., Chen, Z.-Q., Zhang, L., Hu, Z., Li, Z., 2020. Lower Triassic carbonate $\delta^{238}U$ record demonstrates expanded oceanic anoxia during Smithian Thermal Maximum and improved ventilation during Smithian-Spathian boundary cooling event. Palaeogeography, Palaeoclimatology, Palaeoecology 539, 109393.

Figure captions

Fig. 1. Early Triassic (**A**) and present-day (**B**) locations of the western USA basin. **C**. Map of northern Utah showing the location of the two sampled localities.

Fig. 2. Simplified stratigraphic log showing ammonoid occurrences at Lower Weber Canyon (Morgan County, Utah). Stratigraphy follows the main units described by Grosjean et al. (2018).

Fig. 3. Simplified stratigraphic log showing ammonoid occurrences at Thumb Ridge (Tooele County, Utah).

Fig. 4. A–L, P. *Xenoceltites subevolutus*. **M–O**. *Xenoceltites subevolutus* (Xs) and *Pseudosageceras augustum* (Pa). Specimens A–E from bed LWC46, Lower Weber Canyon, Utah, early late Smithian; specimens F–J from bed LWC48, Lower Weber Canyon, Utah, latest Smithian; specimens K–P from bed THU A2, Thumb Ridge, Utah, latest Smithian. A, B: lateral and ventral views of UBGD 32330; C: suture line of UBGD 32330 at H = 15.7 mm; D: UBGD 32331; E: UBGD 32332; F–L: UBGD 32333–32339; M, N: lateral and ventral views of UBGD 32340; O: UBGD 32341; P: UBGD 32342. Black arrows indicate the position of the corresponding ventral view. Scale bars: 10 mm (A, B, D–P), 5 mm (C).

Fig. 5. Scatter diagrams of H, W and U, and H/D, W/D and U/D for *Xenoceltites subevolutus*. Open symbols indicate specimens from Lower Weber Canyon and Thumb Ridge, Utah (n = 7). Grey symbols indicate specimens from Palomino Ridge (data from Jattiot et al., 2017; n = 7) and Crittenden Springs (data from Jenks and Brayard, 2018; n = 32), northeastern Nevada.

Fig. 6. A–R. *Pseudosageceras augustum* from beds LWC48 and LWC49, Lower Weber Canyon, Utah, latest Smithian (A–G) and from bed THU A2, Thumb Ridge, Utah, latest Smithian (H–R). A–C: lateral, ventral and apertural views of UBGD 32343; D–G: UBGD 32344–32347; H, I: lateral and ventral views of UBGD 32348; J: suture line of UBGD 32348 at H = 16.4 mm; K: UBGD 32349; L, M: lateral and ventral views of UBGD 32350; N: UBGD 32351; O, P: lateral and ventral views of UBGD 32352; Q, R: lateral and ventral views of UBGD 32353. Black arrows indicate the position of the corresponding ventral view. The position of the drawn suture line J is indicated by the asterisk Scale bars: 10 mm (A–I, K–R), 5 mm (J).

Fig. 7. Scatter diagrams of H, W and U, and H/D, W/D and U/D for *Pseudosageceras augustum*. Open symbols indicate specimens from Lower Weber Canyon and Thumb Ridge, Utah (n = 7). Grey symbols indicate specimens from Crittenden Springs, northeastern Nevada (data from Jenks and Brayard, 2018; n = 7), South Tibet (data from Brühwiler et al., 2010; n = 2), Spiti (data from Brühwiler et al., 2012a; n = 2) and South China (data from Brayard and Bucher, 2008; n = 31).

Fig. 8. A–Q. *Gurleyites smithi* from bed LWC46, Lower Weber Canyon, Utah, early late Smithian. A, B: Lateral and ventral views of UBGD 32354; C: UBGD 32355; D, E: Lateral and ventral views of UBGD 32356; F: UBGD 32357; G: UBGD 32358; H: Suture line of UBGD 32358 at H = 16.9 mm (note this suture line is asymmetrical with expected ventral axis [blue arrow] shifted on the left side); I–K: UBGD 32359–32361; L: Suture line of UBGD 32361 at H = 23.5 mm (slightly weathered); M: UBGD 32362; N: UBGD 32363; O, P: Lateral and ventral views of UBGD 32364; Q: UBGD 32365. Black arrows indicate the position of the corresponding ventral view. Scale bars: 10 mm (A–G, I–K, M–Q), 5 mm (H, L).

Fig. 9. A–I. *Gurleyites smithi*. **J–N**. *Anasibirites kingianus*. Specimens from bed LWC46, Lower Weber Canyon, Utah, early late Smithian. A–E: specimens illustrating most evolute morphs of *G. smithi* (A, block UBGD 32366 with four specimens illustrating the large intraspecific variation of the species; B, UBGD 32367; C, block UBGD 32368 with one evolute specimen of *G. smithi* and one specimen of *Hemiprionites typus* (H); D, E, lateral and ventral views of UBGD 32369); F–I: lateral views of UBGD 32370–32373; J–L: lateral views of UBGD 32374, 32375 and 32376; M, N: lateral and ventral views of UBGD 32377. Black arrows indicate the position of the corresponding ventral view. Scale bars: 10 mm.

Fig. 10. Scatter diagrams of H, W and U, and H/D, W/D and U/D for *Gurleyites smithi*. Open symbols indicate specimens from Lower Weber Canyon and Thumb Ridge, Utah (n = 25). Grey symbols indicate specimens from Workman Wash (data from Brayard et al., 2020; n = 40), southern Utah, and Palomino Ridge (data from Jattiot et al., 2017; n = 7) and Crittenden Springs (data from Jenks and Brayard, 2018; n = 14), northeastern Nevada. Blue symbols indicate six similarly sized specimens from Lower Weber Canyon that exhibit a much more evolute coiling than other specimens.

Fig. 11. A–Q. *Wasatchites perrini* from bed LWC46, Lower Weber Canyon, Utah, early late Smithian. A, B: lateral and ventral views of UBGD 32378; C: UBGD 32379; D: UBGD 32380; E–G: lateral and ventral views of UBGD 32381; H: UBGD 32382; I: UBGD 32383; J, K: lateral and ventral views of UBGD 32384; L: poorly preserved suture line of UBGD 32384 at H = 15 mm; M: UBGD 32385; N, O: lateral and ventral views of UBGD 32386; P, Q: lateral views of UBGD 32387. Black arrows indicate the position of the corresponding ventral view. Scale bars: 10 mm (A–J, L–Q), 5 mm (K).

Fig. 12. Scatter diagrams of H, W and U, and H/D, W/D and U/D for *Wasatchites perrini*. Open symbols indicate specimens from Lower Weber Canyon, Utah (n = 10). Grey symbols indicate specimens from the Confusion Range (data from Brayard et al., 2013; n = 2), western Utah, and Palomino Ridge (data from Jattiot et al., 2017; n = 4) and Crittenden Springs (data from Jenks and Brayard, 2018; n = 2), northeastern Nevada.

Fig. 13. Scatter diagrams of H, W and U, and H/D, W/D and U/D for *Anasibirites kingianus*. Open symbols indicate specimens from Lower Weber Canyon, Utah (n = 4). Grey symbols

indicate specimens from Palomino Ridge (data from Jattiot et al., 2017; n = 5) and the compilation of measurements from Timor, Salt Range and Spitsbergen (data from Jattiot et al., 2016; n = 903).

Fig. 14. A–R. *Anasibirites multiformis* from bed LWC46, Lower Weber Canyon, Utah, early late Smithian (A–P) and from bed THU A1, Thumb Ridge, Utah, early late Smithian (Q, R). A–N, P: UBGD 32388–32401; O: suture line of UBGD 32401 at H = 15.3 mm; P: UBGD 32402; Q: UBGD 32403; R: suture line of UBGD 32403 at H = 30.1 mm. Scale bars: 10 mm (A–N, P, Q), 5 mm (O, R).

Fig. 15. Scatter diagrams of H, W and U, and H/D, W/D and U/D for *Anasibirites multiformis*. Open symbols indicate specimens from Lower Weber Canyon, Utah (n = 27). Grey symbols indicate specimens from Workman Wash (data from Brayard et al., 2020; n = 14), Palomino Ridge (data from Jattiot et al., 2017; n = 54) and Timor (data from Jattiot et al., 2016; n = 21).

Fig. 16. A–M. *Hemiprionites typus* from bed LWC46, Lower Weber Canyon, Utah, early late Smithian. A–C: blocks UBGD 32404–32406 with several *H. typus* specimens showing the characteristic ventral minute depression (A: *Anasibirites*); D: UBGD 32407; E, F: lateral and ventral views of UBGD 32408; G: UBGD 32409; H, I: lateral and ventral views of UBGD 32410; J: UBGD 32411; K: suture line of UBGD 32411 at H = 10 mm; L: UBGD 32412; M: UBGD 32413. Scale bars: 10 mm (A–J, L, M), 5 mm (K).

Fig. 17. A–K. *Hemiprionites typus*. **L–R**. *Hemiprionites walcotti.* Specimens from bed LWC46, Lower Weber Canyon, Utah, early late Smithian (A–J, L–R) and from bed THU A1,

Thumb Ridge, Utah, early late Smithian (K, with a crenulated venter). A–D: UBGD 32414–32417; E, F: lateral and ventral views of UBGD 32418; G: UBGD 32419; H: suture line of UBGD 32419 at H = 14.4 mm; I: UBGD 32420; J: UBGD 32421; K: UBGD 32422; L, M: lateral and ventral views of UBGD 32423; N: UBGD 32424; O: UBGD 32425; P, Q: lateral and ventral views of UBGD 32426; R: suture line of UBGD 32426 at H = 22 mm. Scale bars: 10 mm (A–G, I–R), 5 mm (H).

Fig. 18. Scatter diagrams of H, W and U, and H/D, W/D and U/D for *Hemiprionites typus*. Open symbols indicate specimens from Lower Weber Canyon, Utah (n = 22). Grey symbols indicate specimens from Workman Wash (data from Brayard et al., 2020; n = 6), southern Utah, Palomino Ridge (data from Jattiot et al., 2017; n = 58) and Crittenden Springs (data from Jenks and Brayard, 2018; n = 23), Nevada, Salt Range (data modified from Brühwiler et al., 2012b; n = 20), Pakistan, and Timor (data from Jattiot et al., 2020; n = 186).

Fig. 19. Scatter diagrams of H, W and U, and H/D, W/D and U/D for *Hemiprionites walcotti*. Open symbols indicate specimens from Lower Weber Canyon and Thumb Ridge, Utah (n = 5). Grey symbols indicate specimens from Workman Wash (data from Brayard et al., 2020; n = 5), southern Utah, Palomino Ridge (data from Jattiot et al., 2017; n = 26) and Crittenden Springs (data from Jenks and Brayard, 2018; n = 2), Nevada, and Timor (data from Jattiot et al., 2020; n = 11).

Fig. 20. Biogeographical distribution of middle and late Smithian ammonoids within three main areas: South China, the western USA basin and the Northern Indian Margin. Genera reported in this study are highlighted in bold. Abbreviations: mSm: middle Smithian = UAZ4 in the western USA basin; late Sm: late Smithian; lS1: early late Smithian = UAZ5 in the

western USA basin = UAZ S-13 in the Northern Indian Margin = *Anasibirites* beds *s.s.* in South China; lS2: latest Smithian = UAZ6 in the western USA basin = UAZ S-14 in the Northern Indian Margin = upper *Anasibirites* beds in South China. For correlations between biostratigraphical scales, see Brühwiler et al. (2011), Jenks et al. (2015), Jattiot et al. (2017) and Jenks and Brayard (2018).

Appendix A. Supplementary information.

Shell measurements (D: diameter, H: height W: width, and U: umbilical diameter) for some late Smithian ammonoids from Lower Weber Canyon and Thumb Ridge, Utah. Some measurements for these taxa sampled elsewhere are also given for comparison.

Table S1: *Xenoceltites subevolutus.*

Table S2: *Pseudosageceras augustum.*

Table S3: *Gurleyites smithi.*

Table S4: *Wasatchites perrini.*

Table S5: *Anasibirites kingianus.*

Table S6: *Anasibirites multiformis.*

Table S7: *Hemiprionites typus.*

Table S8: *Hemiprionites walcotti.*

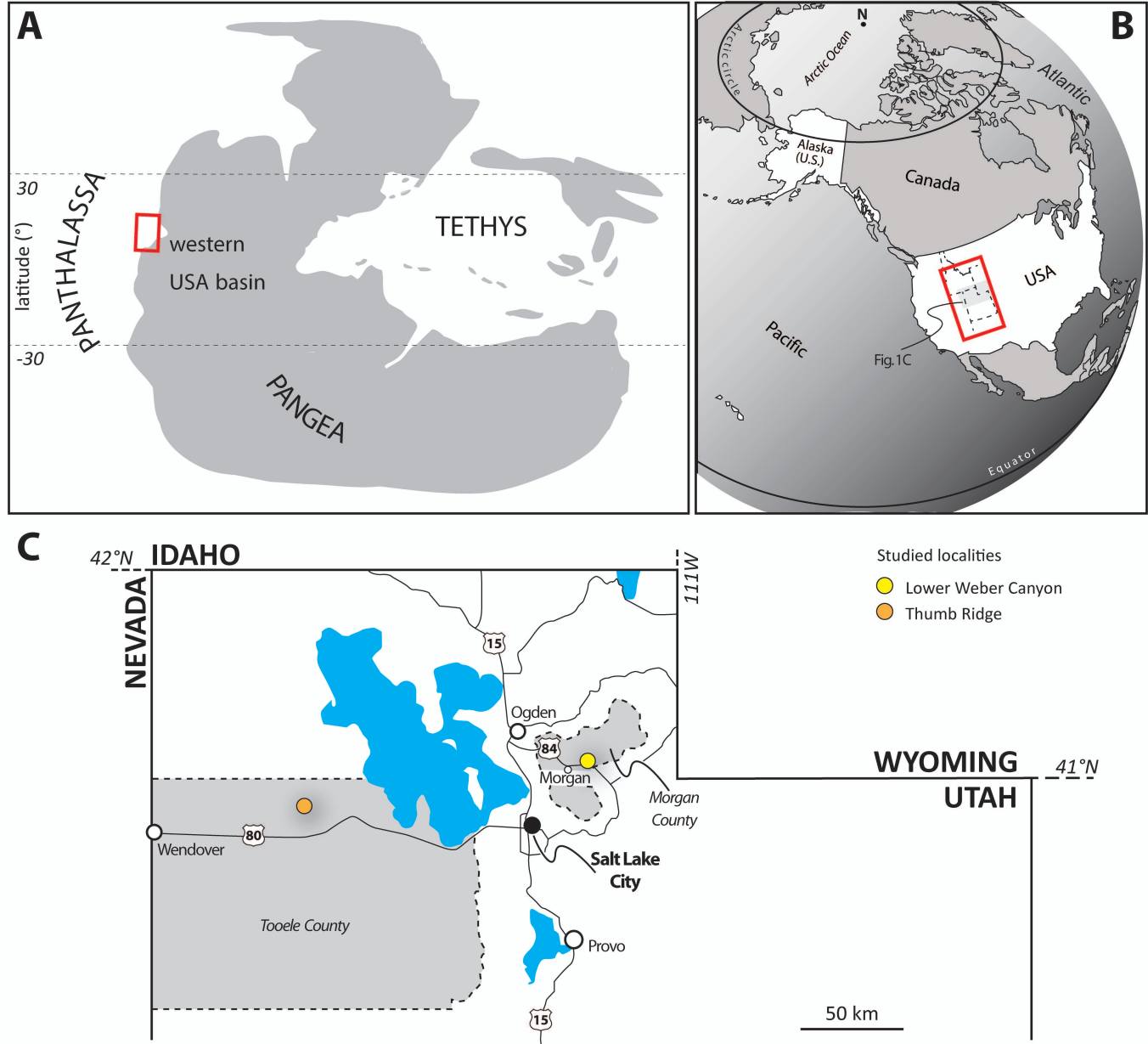
A
30
latitude (°)
-30
PANTHALASSA
western
USA basin
TETHYS
PANGEA
B
N
Arctic circle
Arctic Ocean
Atlantic
Alaska (U.S.)
Canada
USA
Pacific
Fig.1C
Equator
C
42°N
IDAHO
NEVADA
111W
WYOMING
UTAH
41°N
Studied localities
Lower Weber Canyon
Thumb Ridge
15
Ogden
84
Morgan
Morgan County
80
Wendover
Salt Lake City
Tooele County
Provo
15
50 km

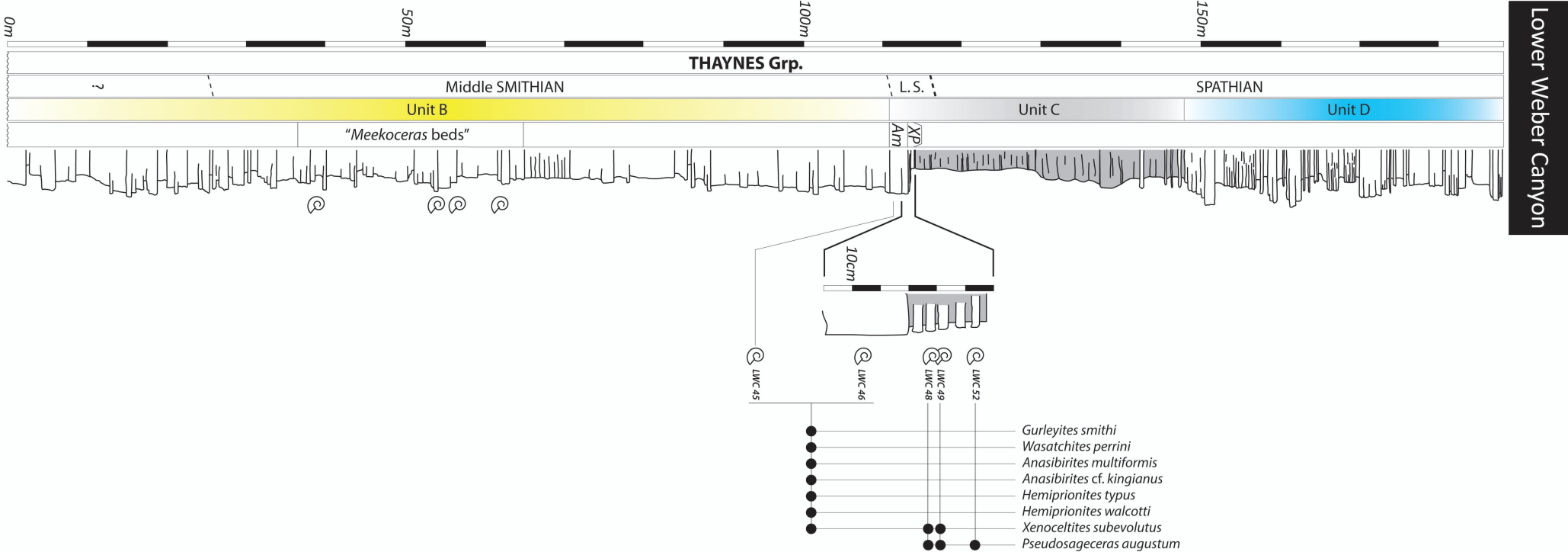
Lower Weber Canyon
0m
50m
100m
150m
THAYNES Grp.
?
Middle SMITHIAN
L.S.
SPATHIAN
Unit B
Unit C
Unit D
"Meekoceras beds"
Am
XP
10cm
LWC 45
LWC 46
LWC 48
LWC 49
LWC 52
Gurleyites smithi
Wasatchites perrini
Anasibirites multiformis
Anasibirites cf. kingianus
Hemiprionites typus
Hemiprionites walcotti
Xenoceltites subevolutus
Pseudosageceras augustum

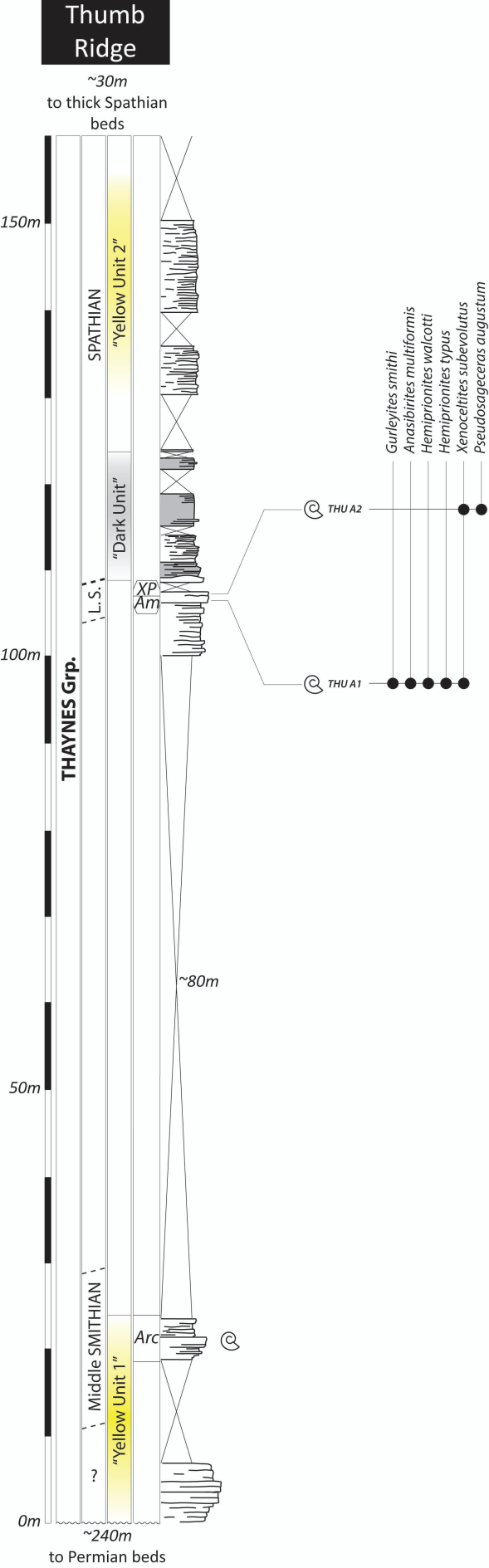
Thumb Ridge
~30m
to thick Spathian beds
150m
100m
50m
0m
~240m
to Permian beds
THAYNES Grp.
SPATHIAN
Middle SMITHIAN
"Yellow Unit 2"
"Dark Unit"
"Yellow Unit 1"
L.S.
?
XP
Am
Arc
~80m
THU A2
THU A1
Gurleyites smithi
Anasibirites multiformis
Hemiprionites walcotti
Hemiprionites typus
Xenoceltites subevolutus
Pseudosageceras augustum

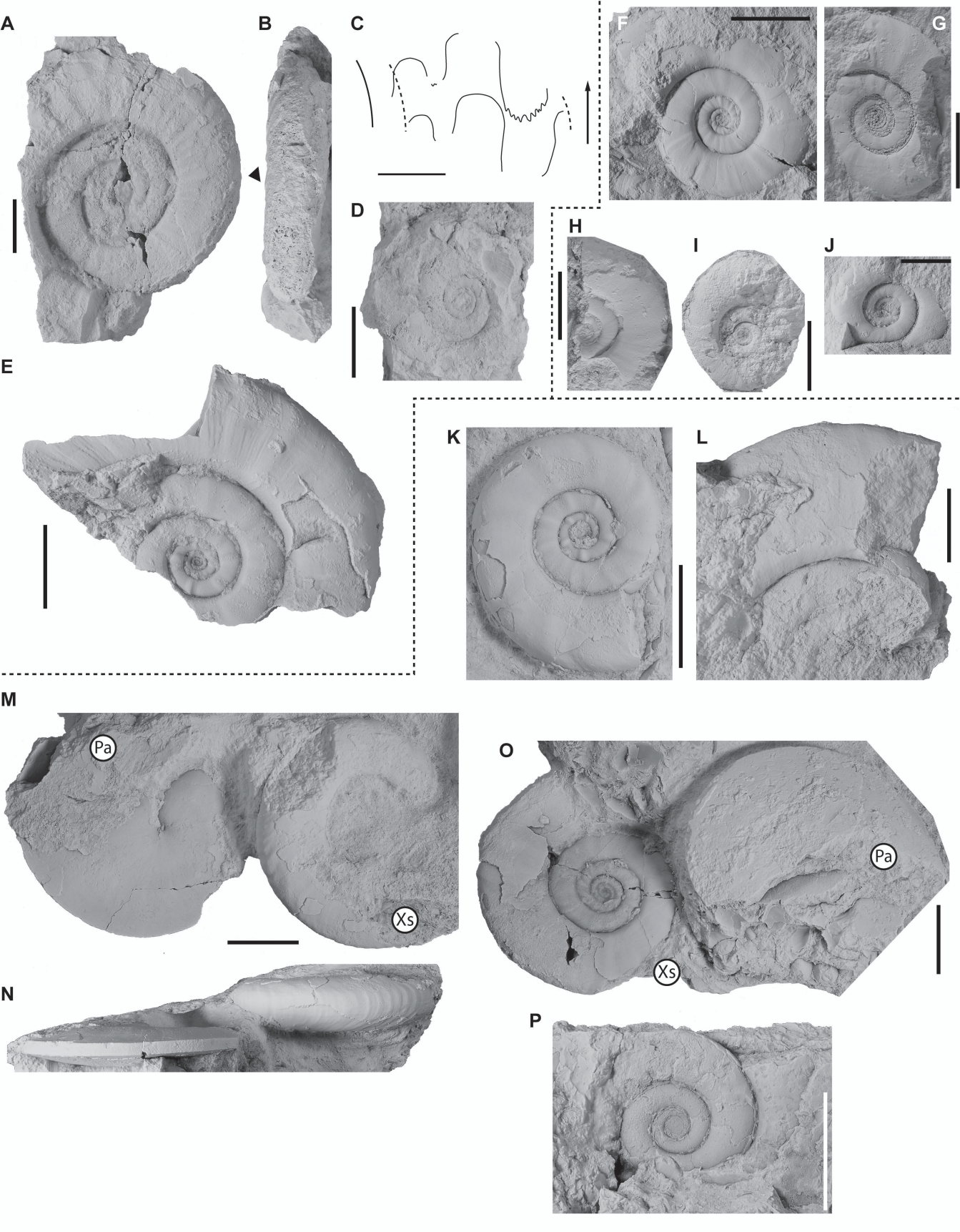
A
B
C
D
E
F
G
H
I
J
K
L
M
Pa
Xs
N
O
Pa
Xs
P

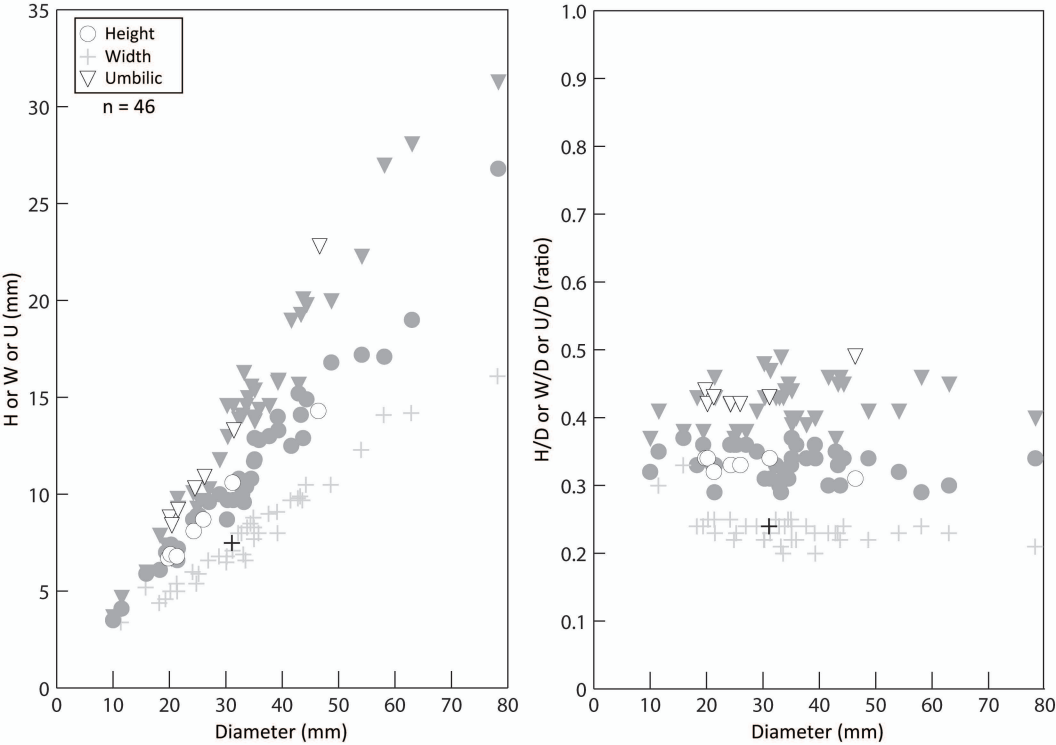
Height
Width
Umbilic
n = 46
H or W or U (mm)
Diameter (mm)
H/D or W/D or U/D (ratio)
Diameter (mm)

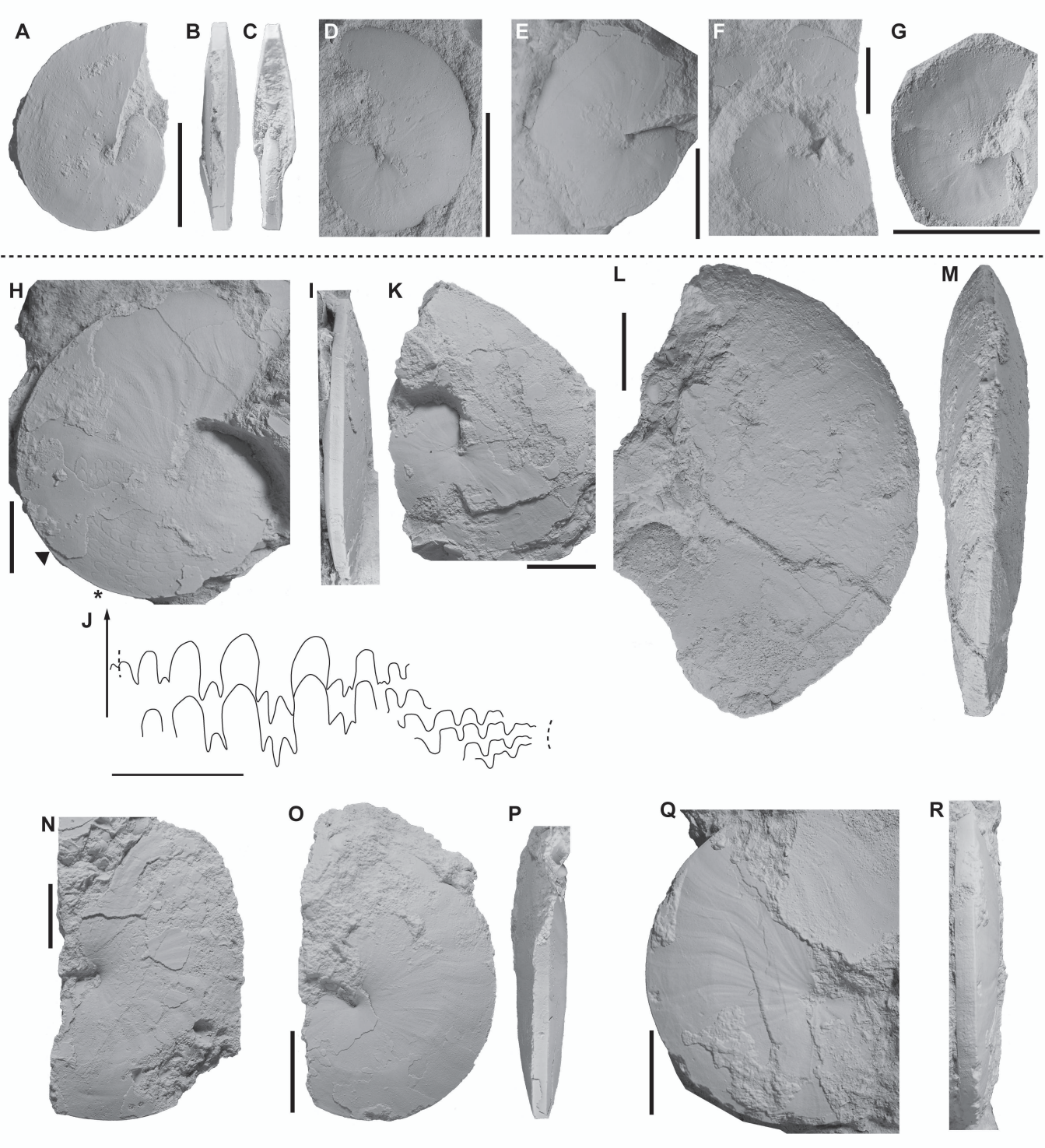
A
B
C
D
E
F
G
H
I
K
L
M
J
N
O
P
Q
R

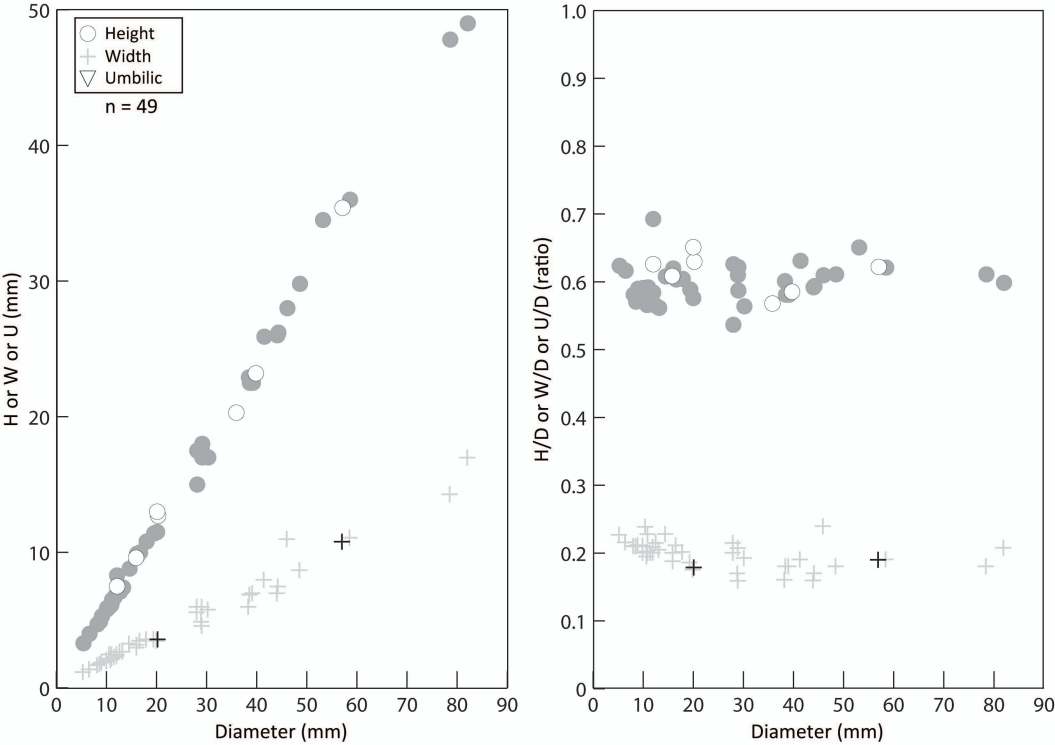
Height
Width
Umbilic
n = 49
H or W or U (mm)
Diameter (mm)
H/D or W/D or U/D (ratio)
Diameter (mm)

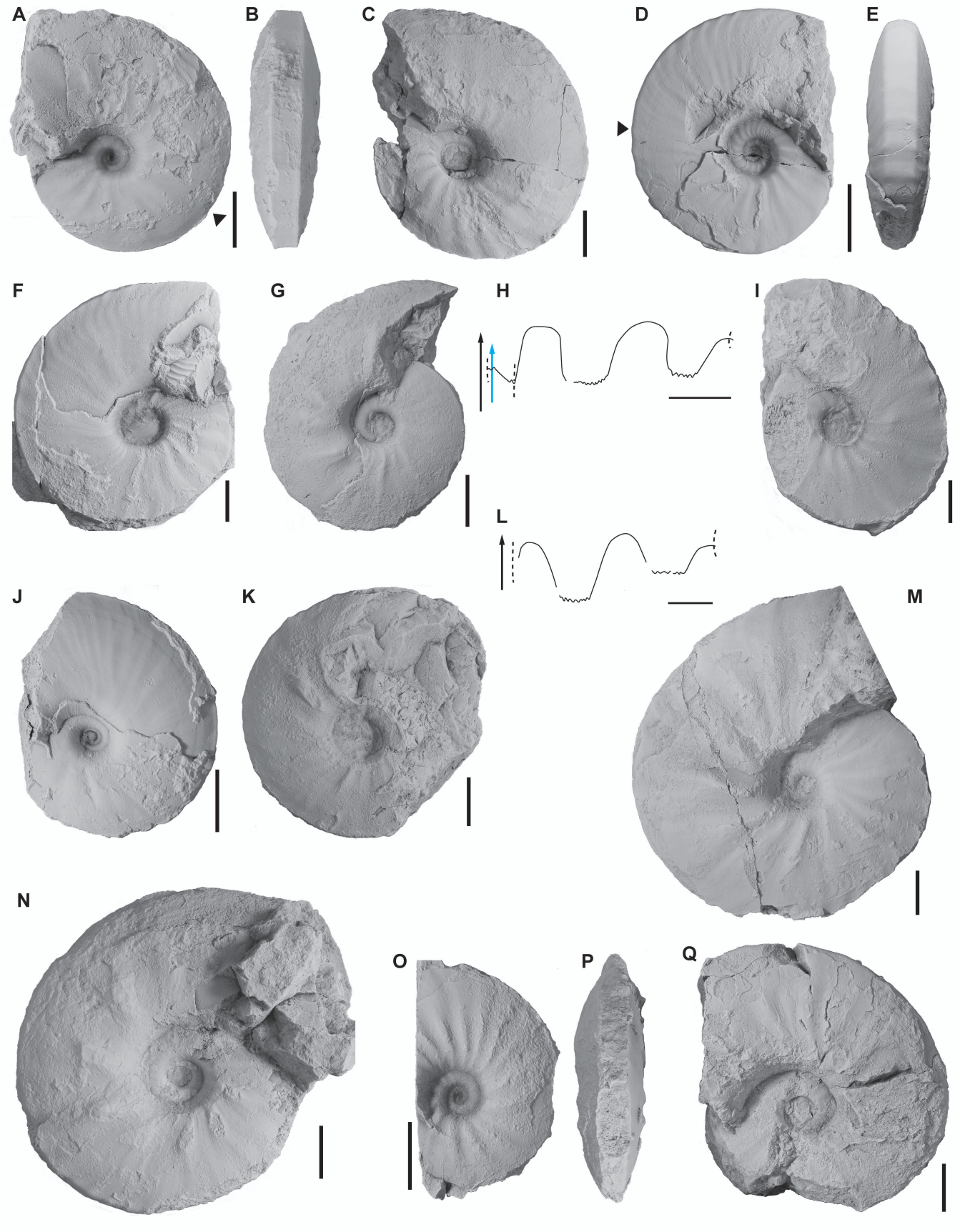
A
B
C
D
E
F
G
H
I
L
J
K
M
N
O
P
Q

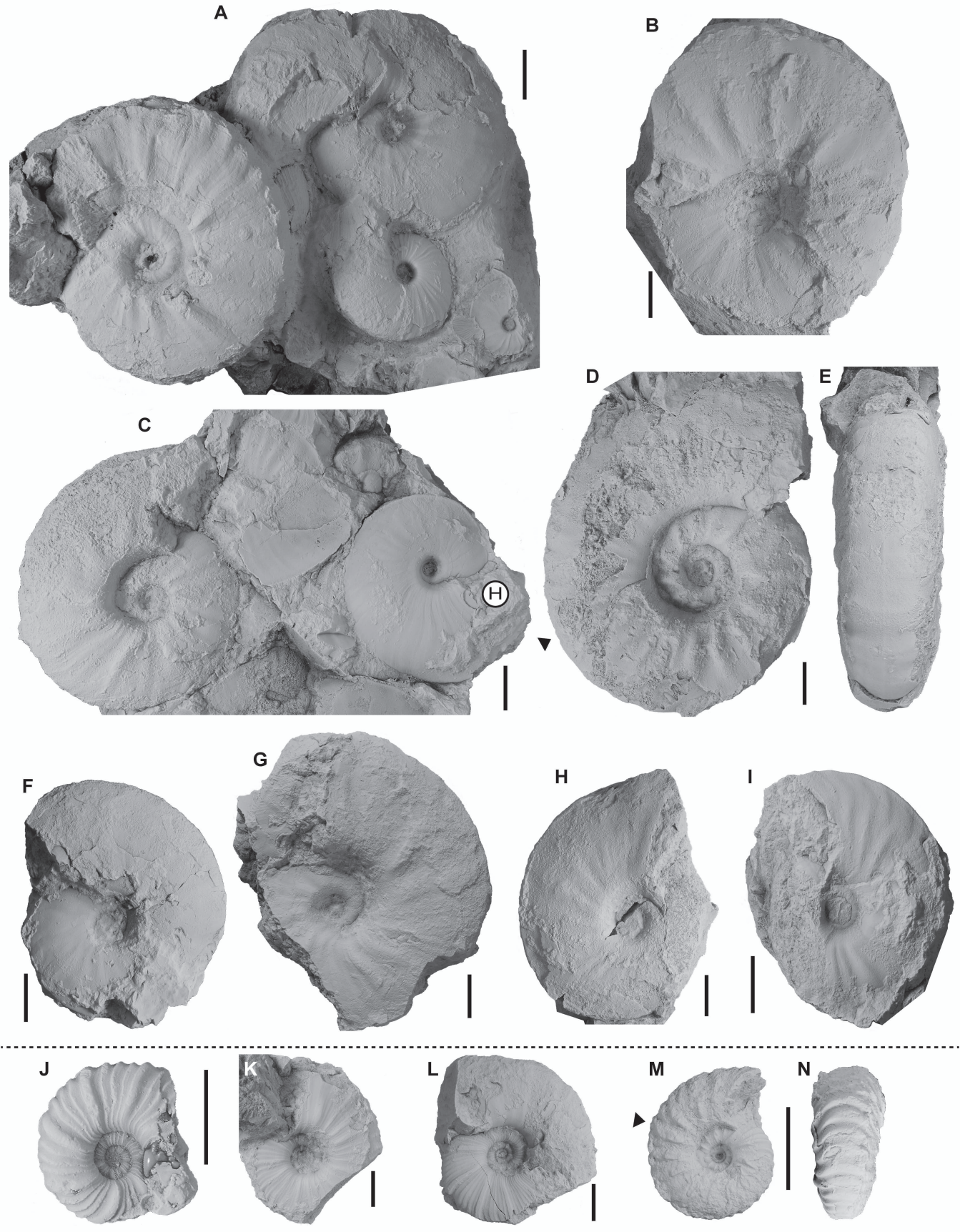
A
B
C
H
D
E
F
G
H
I
J
K
L
M
N

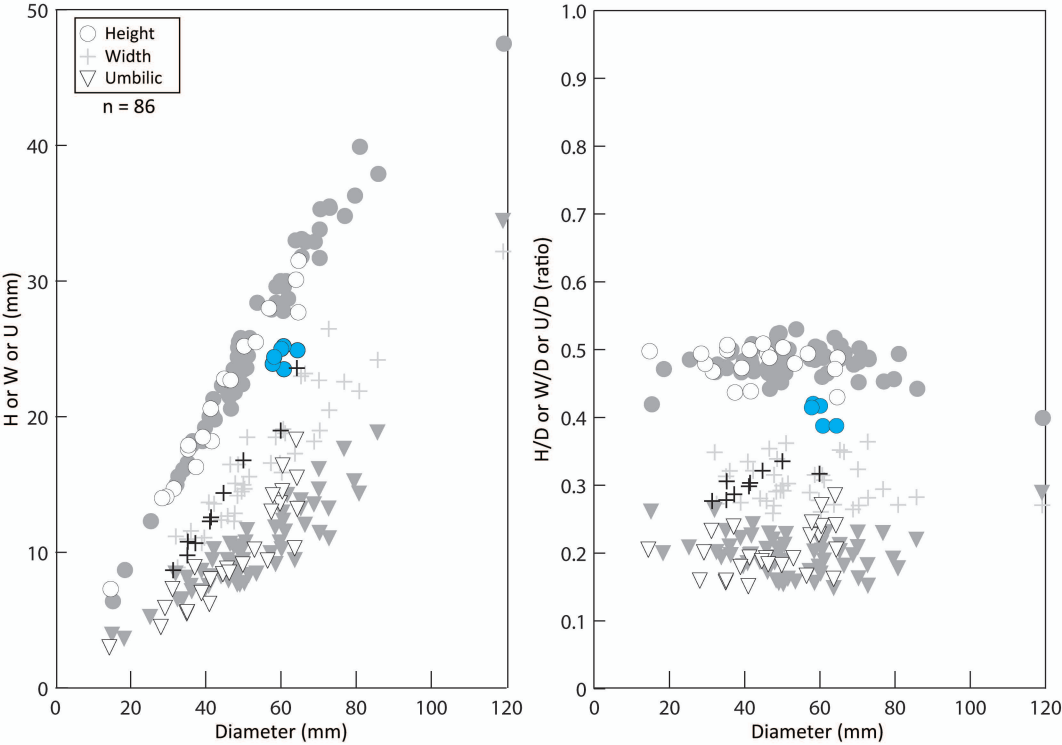
Height
Width
Umbilic
n = 86
H or W or U (mm)
Diameter (mm)
H/D or W/D or U/D (ratio)
Diameter (mm)

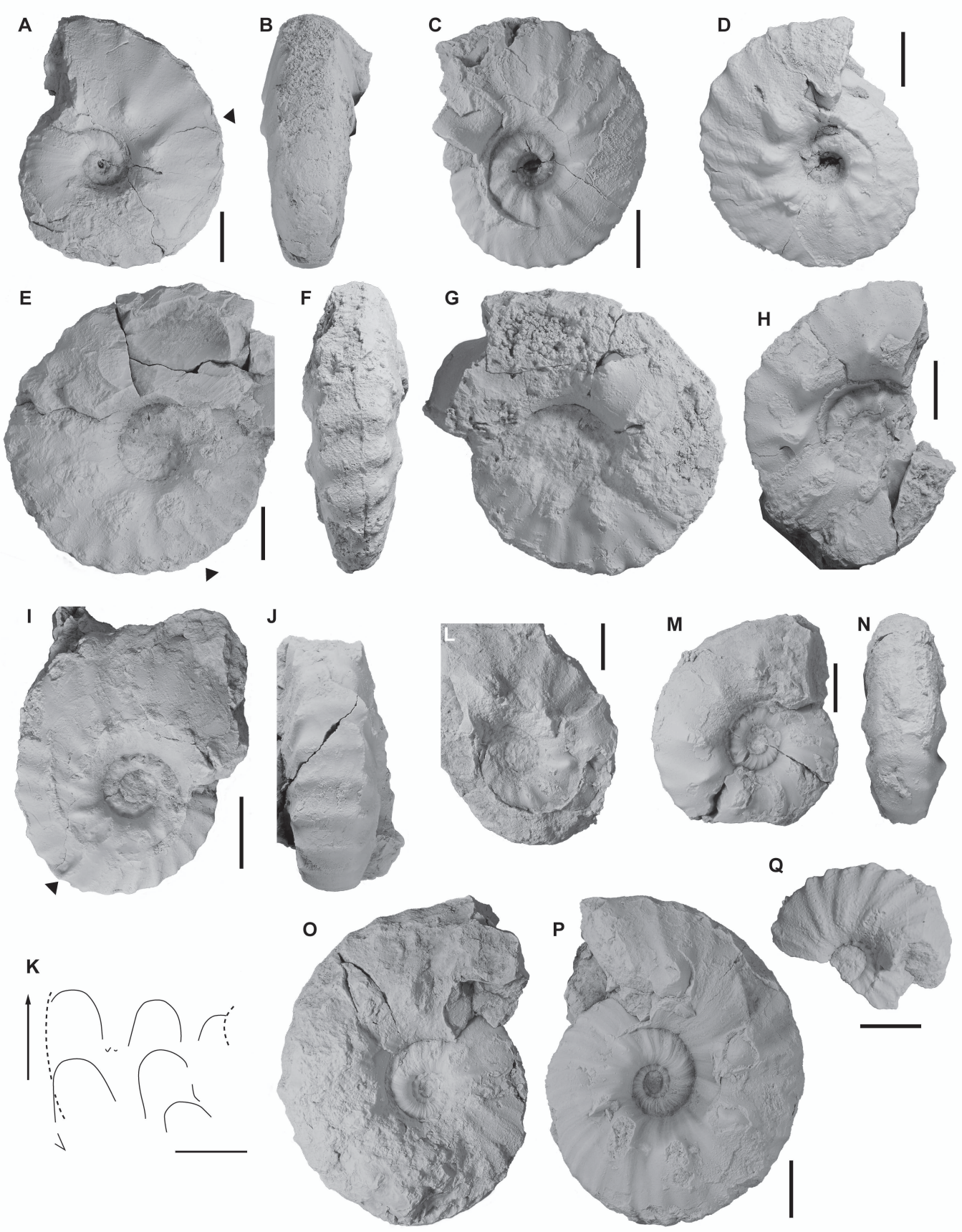
A
B
C
D
E
F
G
H
I
J
L
M
N
Q
O
P
K

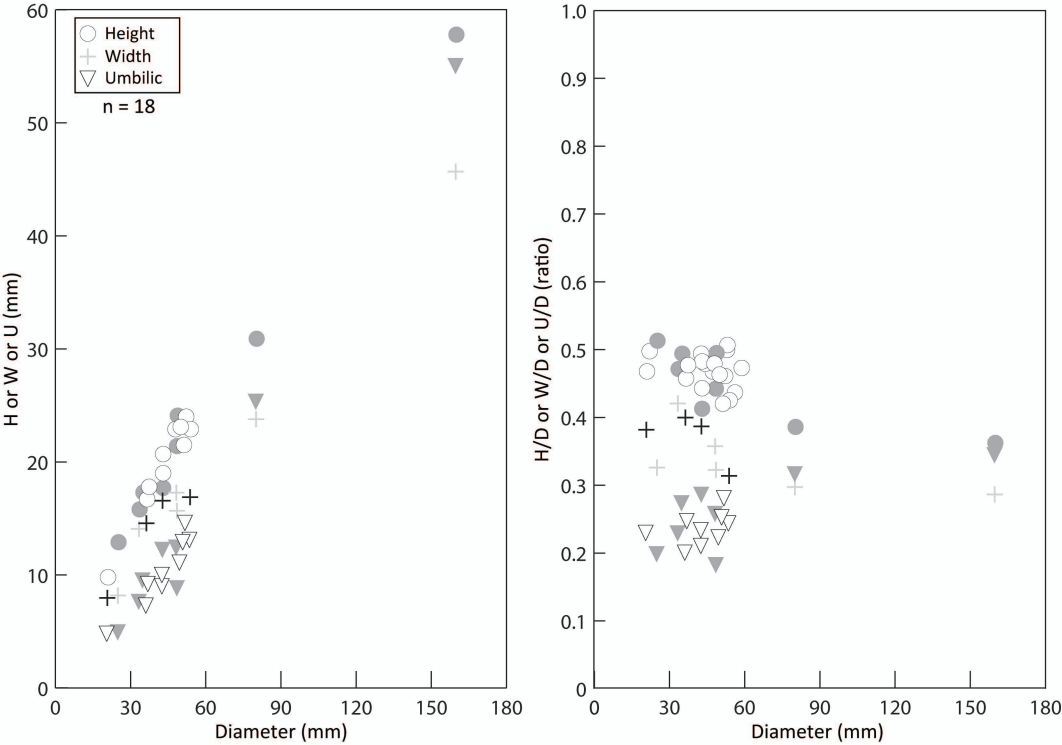
Height
Width
Umbilic
n = 18
H or W or U (mm)
Diameter (mm)
H/D or W/D or U/D (ratio)
Diameter (mm)

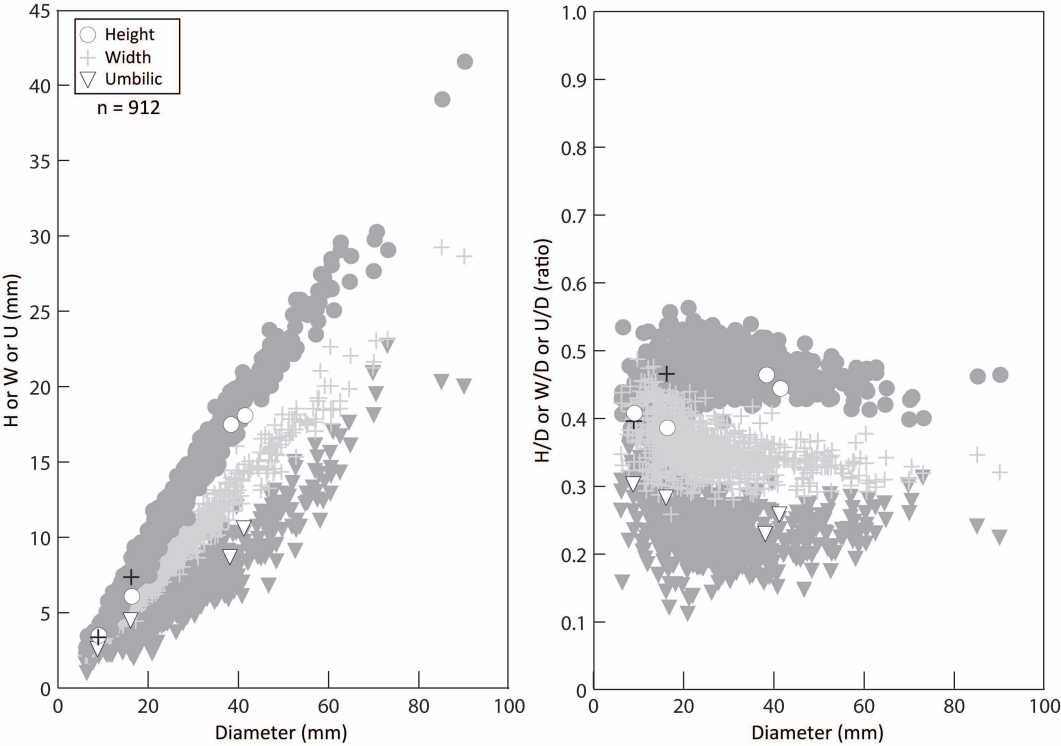
Height
Width
Umbilic
n = 912
H or W or U (mm)
Diameter (mm)
H/D or W/D or U/D (ratio)
Diameter (mm)

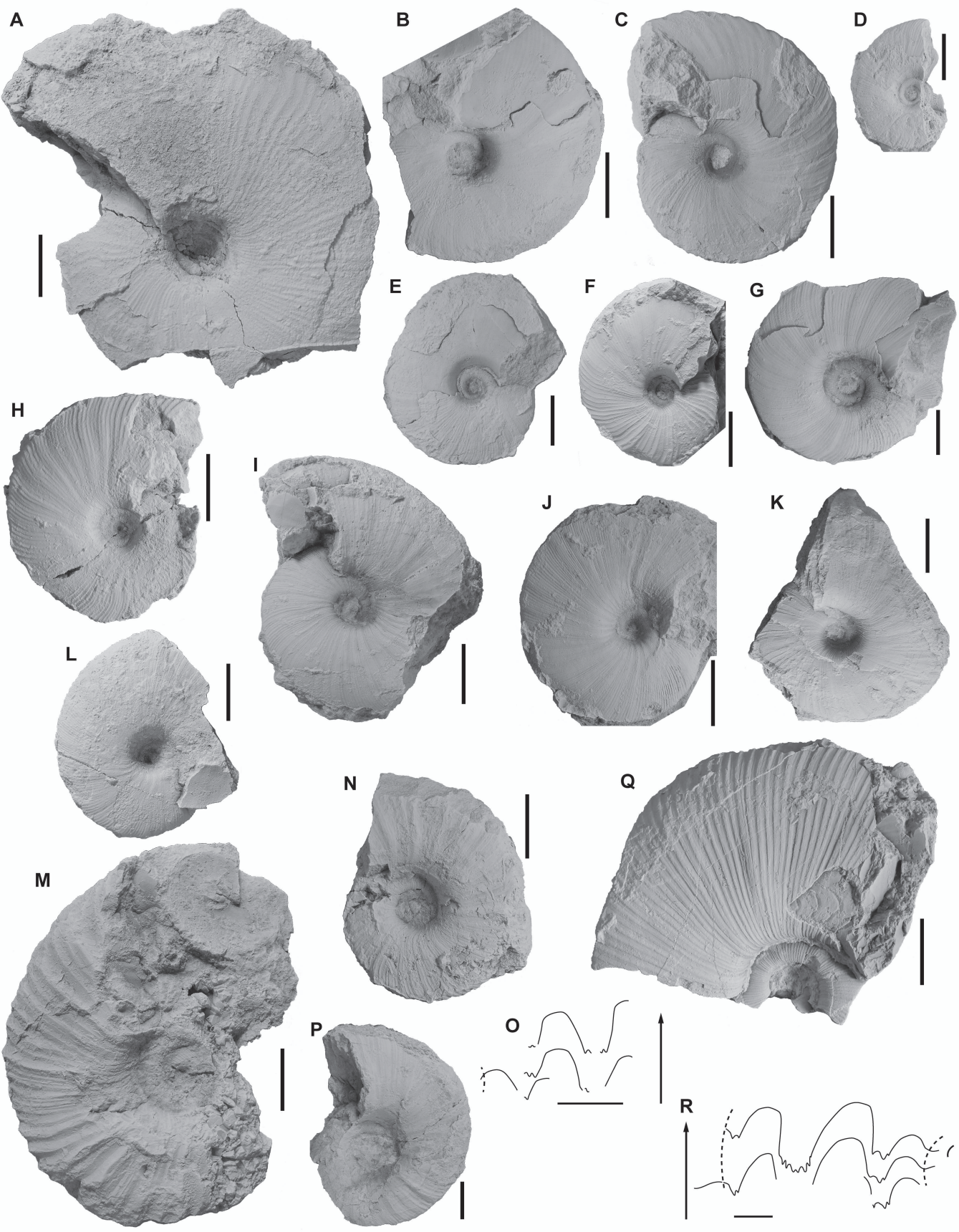
A
B
C
D
E
F
G
H
I
J
K
L
M
N
O
P
Q
R

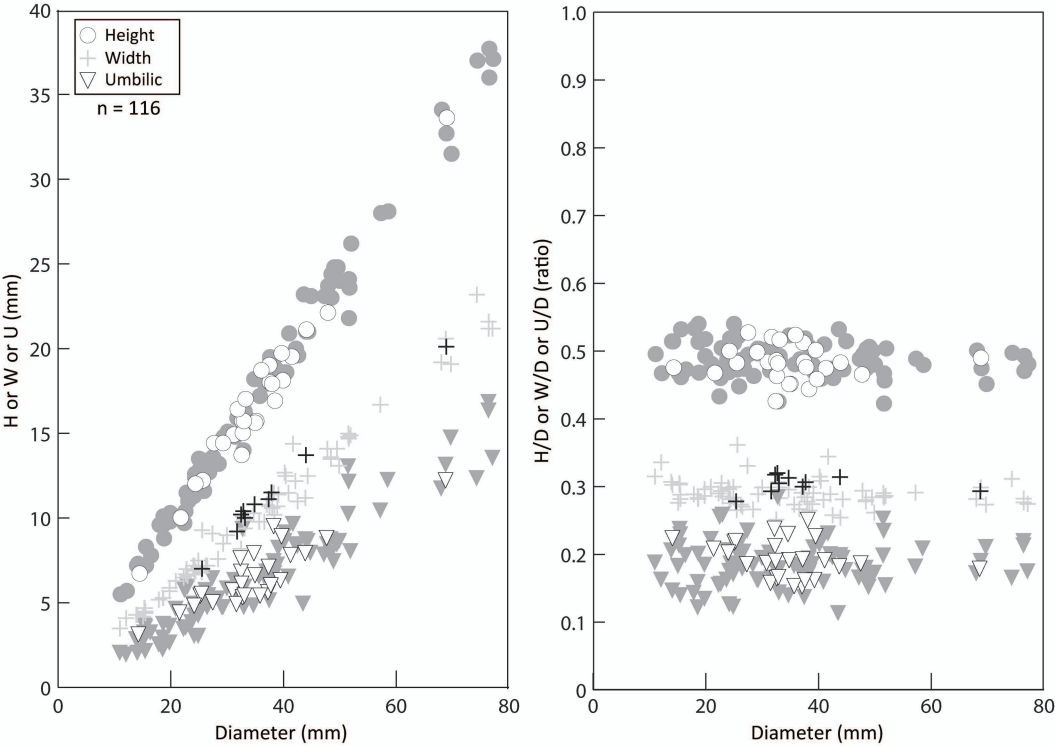
Height
Width
Umbilic
n = 116
H or W or U (mm)
Diameter (mm)
H/D or W/D or U/D (ratio)
Diameter (mm)

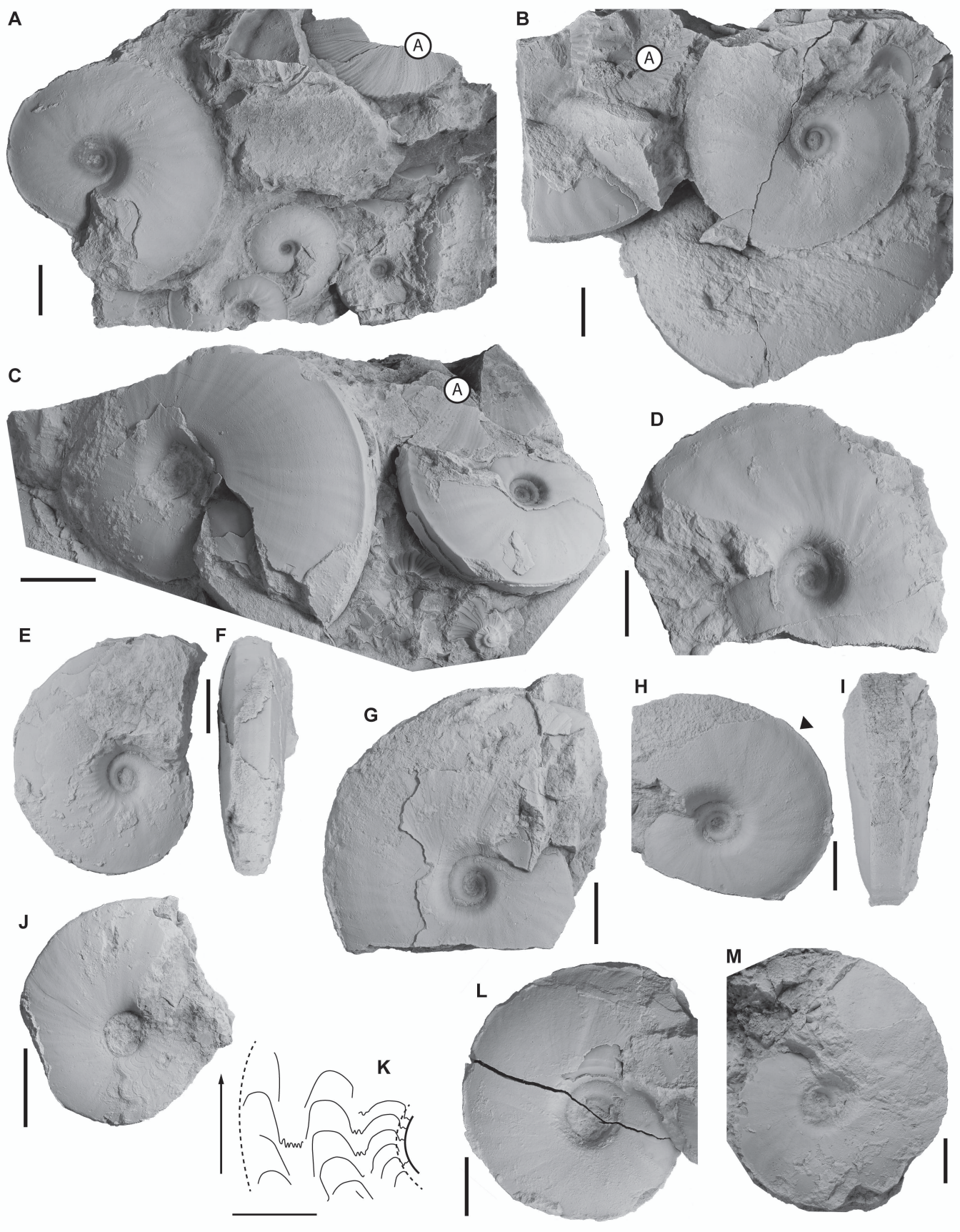
A
A
B
A
C
A
D
E
F
G
H
I
J
K
L
M

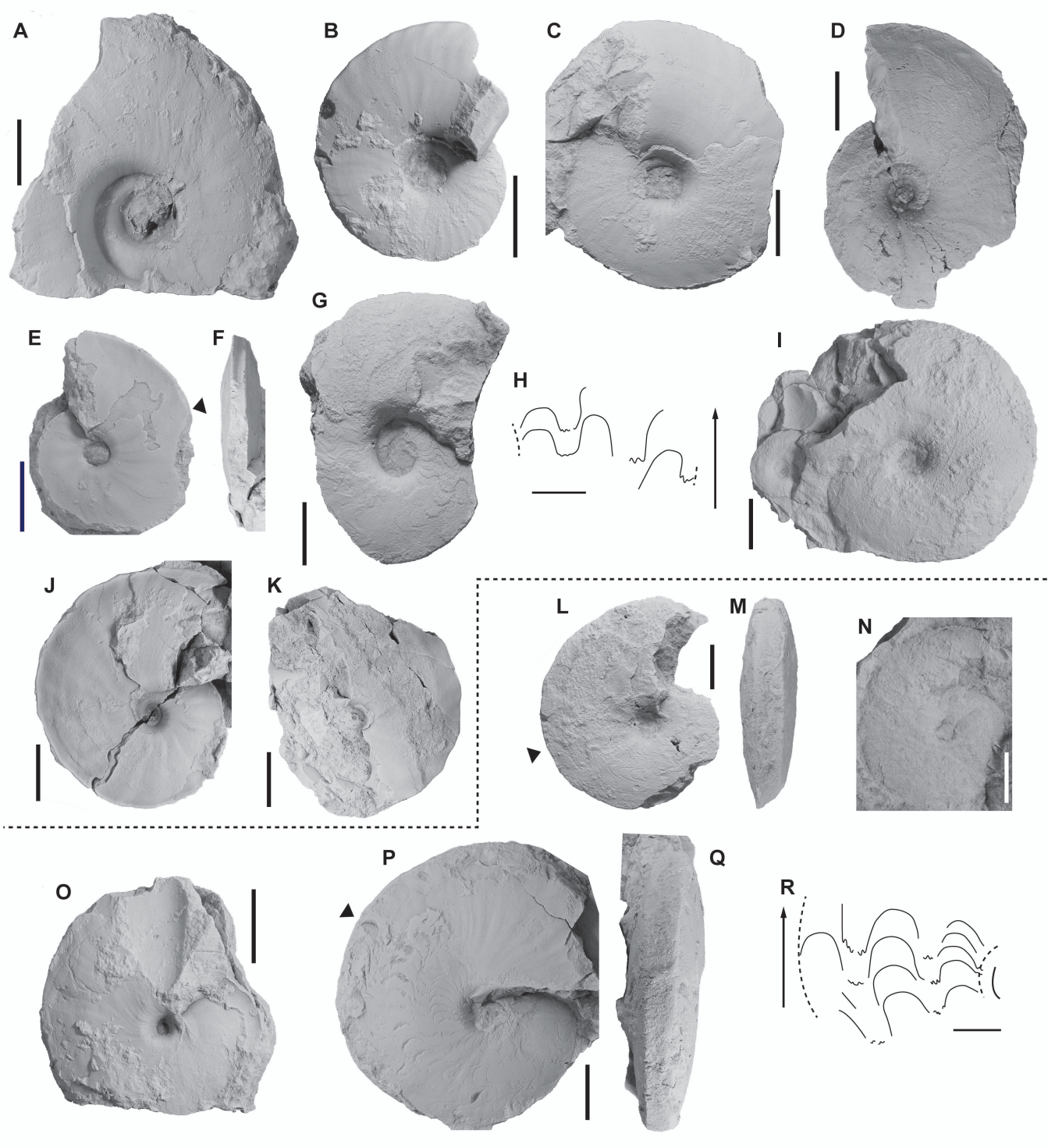
A
B
C
D
E
F
G
H
I
J
K
L
M
N
O
P
Q
R

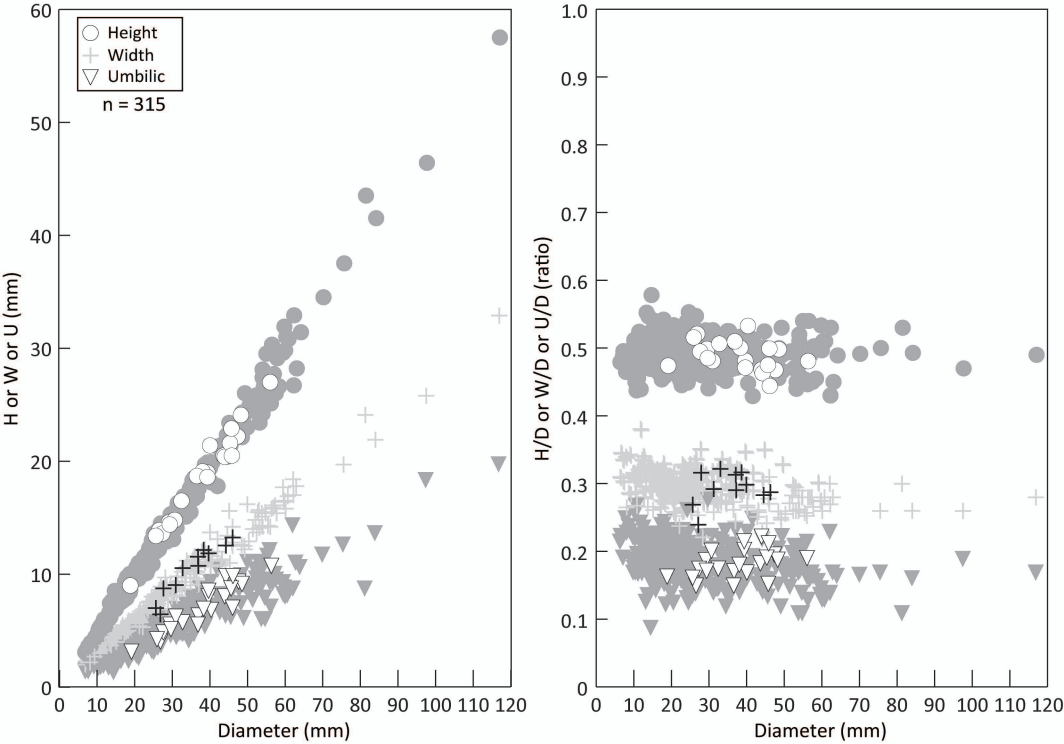
Height
Width
Umbilic
n = 315
H or W or U (mm)
Diameter (mm)
H/D or W/D or U/D (ratio)
Diameter (mm)

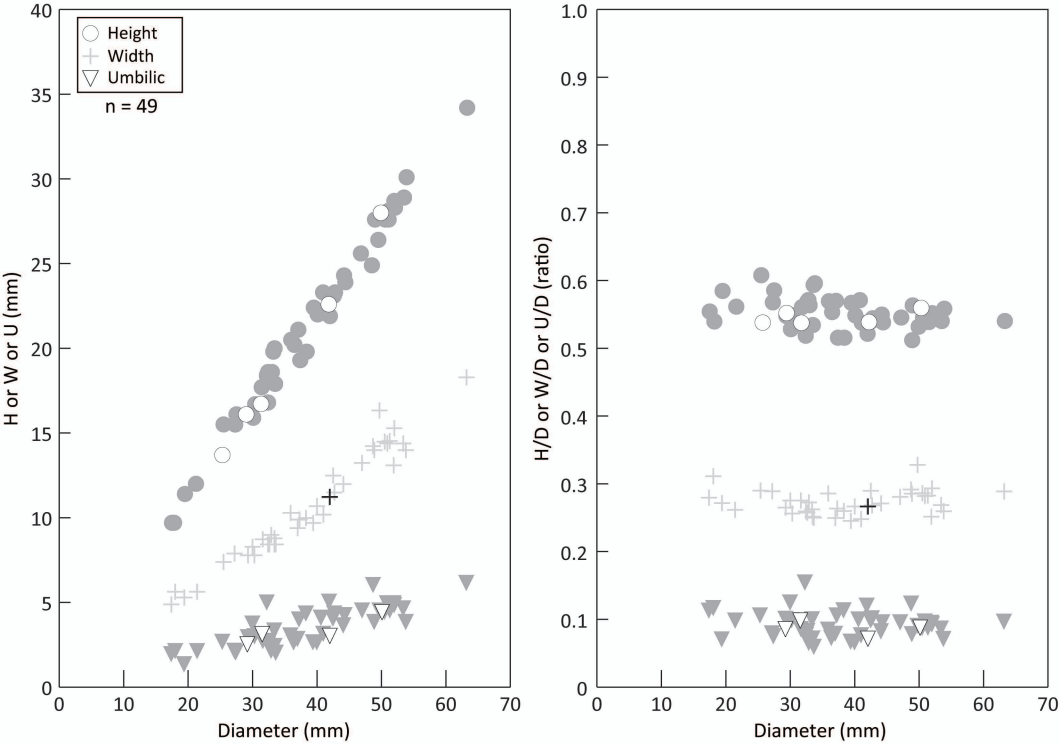
Height
Width
Umbilic
n = 49
H or W or U (mm)
Diameter (mm)
H/D or W/D or U/D (ratio)
Diameter (mm)

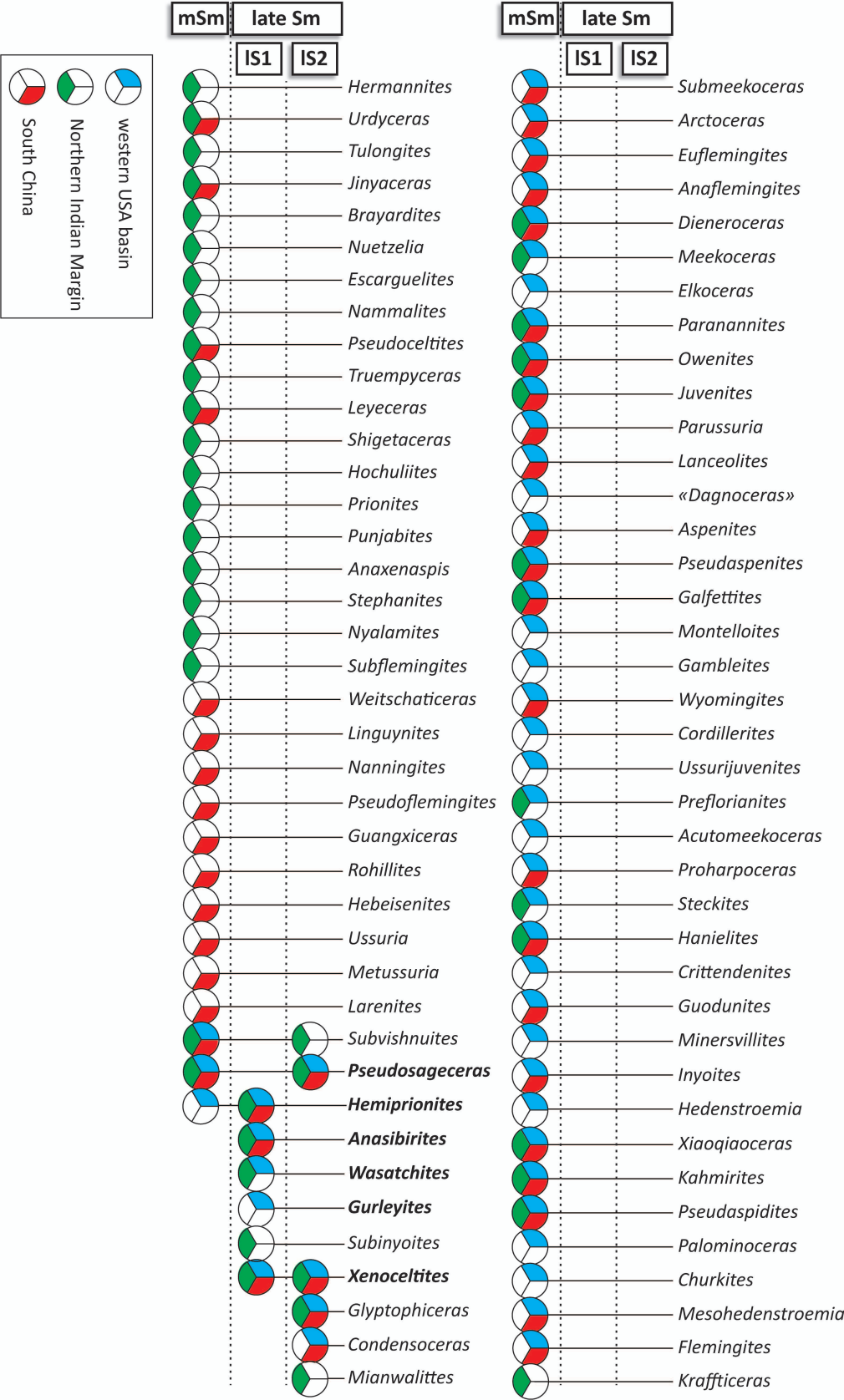
South China
Northern Indian Margin
western USA basin
mSm
late Sm
IS1
IS2
Hermannites
Urdyceras
Tulongites
Jinyaceras
Brayardites
Nuetzelia
Escarguelites
Nammalites
Pseudoceltites
Truempyceras
Leyeceras
Shigetaceras
Hochuliites
Prionites
Punjabites
Anaxenaspis
Stephanites
Nyalamites
Subflemingites
Weitschaticeras
Linguynites
Nanningites
Pseudoflemingites
Guangxiceras
Rohillites
Hebeisenites
Ussuria
Metussuria
Larenites
Subvishnuites
Pseudosageceras
Hemiprionites
Anasibirites
Wasatchites
Gurleyites
Subinyoites
Xenoceltites
Glyptophiceras
Condensoceras
Mianwalittes
mSm
late Sm
IS1
IS2
Submeekoceras
Arctoceras
Euflemingites
Anaflemingites
Dieneroceras
Meekoceras
Elkoceras
Paranannites
Owenites
Juvenites
Parussuria
Lanceolites
«Dagnoceras»
Aspenites
Pseudaspenites
Galfettites
Montelloites
Gambleites
Wyomingites
Cordillerites
Ussurijuvenites
Preflorianites
Acutomeekoceras
Proharpoceras
Steckites
Hanielites
Crittendenites
Guodunites
Minersvillites
Inyoites
Hedenstroemia
Xiaoqiaoceras
Kahmirites
Pseudaspidites
Palominoceras
Churkites
Mesohedenstroemia
Flemingites
Kraffticeras